# RADON ($^{222}$Rn) LEVELS IN GROUND WATERS FROM MUTOMO AREA, IN KITUI COUNTY

`

**ABEL MUTAMBU**
**I64/KIT/20646/2015**

**A Research Thesis Submitted in Partial Fulfillment of the Requirements for the Degree of Master of Science in Physics of South Eastern Kenya University**

**2022**

## DECLARATION

I declare that this research thesis is my original work and has never been presented in any other university for any other award.

Signature……. Date……..

**Abel Mutambu**

**I64/KIT/20646/2015**

## SUPERVISOR'S APPROVAL

We confirm that this thesis has been prepared by the candidate and is being submitted for examination with our approval as University Supervisors.

Signature …… Date……....

**Dr. Mugambi J. Linturi**

**Department of Physical Sciences**

**South Eastern Kenya University**

**P.O BOX 170**

**Kitui, Kenya.**

Signature …… Date……..

**Dr. Jeremiah Kebwaro**

**Department of Physical Sciences**

**Karatina University**

**P.O BOX 1957**

**Karatina, Kenya.**

## ACKNOWLEDGMENT

I owe much gratitude to my supervisors Dr. Linturi J. Mugambi and Dr. Jeremiah M. Kebwaro for their invaluable input in the entire research due to their several, but necessary corrections during the proposal and thesis development.

Special thanks to my dad Joshua Mutambu, my mum Angeline Mutambu and my dear siblings, their encouragement during difficult times is highly appreciated, may God bless you.

Special gratitude is to the Water Resource Authority (WRA) for their assistance during field water samples collection, preparation and in-situ measurements. Thanks to the Ministry of Mining and Petroleum, the Republic of Kenya for allowing me to use their Laboratory during the pre-counting stages. Institute for Nuclear Science and Technology of the University of Nairobi is highly acknowledged for the provision of gamma-ray spectrometer used during analyses of radium in sediment samples, it cannot go unmentioned that their hospitality and generosity of ideas made my visit in their laboratory comfortable particularly by inducting me to the necessary software used for spectral acquisition and analyses.

Above all, I thank the almighty God for His grace, providence, mercies, strength, love, and kindness that is better than life. *"I will give thanks to you O Lord my God, with my whole heart, I will glorify your name forever".*

(**Psalms 86:12**).

## DEDICATION

I do wish to dedicate this part of my work to my wife Faith Katee and my two kids, Bennie Joshua and Katheryn Katanu.

## TABLE OF CONTENTS

**Declaration** ..... **ii**

**Acknowledgment** ..... **iii**

**Dedication** ..... **iv**

**Table of Contents** ..... **v**

**List of Tables** ..... **viii**

**List of Figures** ..... **ix**

**List of Appendices** ..... **xi**

**Abbreviations and Acronyms** ..... **xii**

**Abstract** ..... **xiii**

**CHAPTER ONE**

**1.0 Introduction** ..... 1

1.1 Background to the Study ..... 1

1.2 Statement of the Problem ..... 4

1.3 Objectives of the Study ..... 4

1.3.1 Main Objective of the Study ..... 4

1.3.2 Specific Objectives of the Study ..... 4

1.4 Research Questions ..... 4

1.5 Justification of the Study ..... 5

1.6 Scope and Delimitations of the Study ..... 5

**CHAPTER TWO**

**2.0 Theoretical Considerations** ..... 7

2.1 Radioactivity from Natural Sources ..... 7

2.2 Activity of Radionuclides ..... 8

2.3 Theory of Alpha Emission ..... 9

2.4 Alpha Interaction with Detector ..... 10

2.5 Radiation Interaction with Matter ..... 12

2.5.1 Compton ..... 12

2.5.2 Photoelectric Absorption ..... 13

2.5.3 Pair Production ..... 14

2.6 Radioactive Equilibrium .....15

**CHAPTER THREE**

**3.0 Literature Review** .....18

3.1 Introduction.....18

3.2 Surveys on Radon Outside Kenya .....18

3.3 Radon Surveys in Kenya.....20

3.4 Natural Radioactivity of Sediments.....21

**CHAPTER FOUR**

**4.0 Materials and Methods**.....25

4.1 Study Area .....25

4.2 Materials used in Measurement of Radon in Water.....27

4.3 Collection of Water Samples .....27

4.4 RAD 7 Alpha Detector.....28

4.5 RAD 7 Detector Characterizations .....29

4.6 Radon Measurement using RAD 7 Detector .....30

4.7 Radon Analysis .....31

4.7.1 Radon Activity Concentration (Bq $m^{-3}$)…… …….....31

4.7.2 Mean Annual Effective Dose…….....32

4.7.3 Water to Air Dose Distribution…….....32

4.8 Sediment Sample Collection and Analysis .....32

4.8.1 Materials…….....32

4.8.2 Collection of Sediment Samples…….33

4.8.3 Sample preparation…….33

4.9 HPGe Detector: Operational Characterization.....34

4.9.1 Energy Calibration…….....34

4.9.2 Detector Efficiency (ε)…… ……...35

4.9.3 Detector Resolution……36

4.9.4 Background Correction……...36

4.10 Sediments Dosimetric Quantities.....36

4.10.1 Activity Concentration ($A_c$)……..…….....37

4.10.2 Absorbed Dose (D)…… …….....37
4.10.3 Radium Equivalent ($Ra_{eq}$)…… …….....38
4.10.4 Radon Equivalent ($Rn_{eq}$)…… ……...38

**CHAPTER FIVE**

**5.0 Results and Discussion**.....39
5.1 Introduction.....39
5.2 Analysis of Water Samples.....39
5.2.1 Radon Concentration in Water…….……..39
5.2.2 Annual Indoor Effective Dose from Water……....42
5.2.3 Water to Air Dose Distribution.....45
5.3 Sediments Analyses .....47
5.3.1 Detector Energy Calibration……..47
5.3.2 Detector Efficiency…….....48
5.3.3 Detector Resolution……...49
5.3.4 Background Corrections…….....51
5.4 Analyses of Sediments Samples. .....…….52
5.4.1 Activity Concentration (A) ……53
5.4.2 Absorbed Dose(D)…… …….....55
5.4.3 Annual Effective Dose Rate……..56
5.4.4 Radium equivalent ($Ra_{eq}$)…… ……..59
5.5 Correlation between $^{226}Ra$ in Sediments vs. $^{222}Rn$ in Water .....…62
5.6 Comparison of Present Work Findings with Previous Studies.....63

**CHAPTER SIX**

**6.0 Conclusion and Recommendation**.....65
6.**1** Conclusions.....65
6.2 Recommendations.....66
**References**.....68

## LIST OF TABLES


Table 1.1: Reference levels for various quantities and corresponding recommending body……..…3

Table 4.1: Shows a summary of sampled GPS locations and elevations……27

Table 5.1: Radon concentration in kBq/$m^3$ from various water samples……40

Table 5.2: Indoor annual effective dose rate emanating from water Sampled from various water sources ……... 43

Table 5.3: Water to air dose distribution from various sources..... 46

Table 5.4: The polynomial and its fit parameters used for detector energy Calibration…… 48

Table 5.5: The Gaussian fit and fit parameters used to calculate the detector resolution……...50

Table 5.6: Activity Concentration of $^{226}$Ra, $^{232}$Th and $^{40}$K in sediments samples from the basement of shallow wells and boreholes……..……... 53

Table 5.7: Absorbed doses from sediments samples collected from shallow boreholes ……..55

Table 5.8: Annual effective dose rate estimated from sediments collected from the sampled basement of shallow boreholes in Kitui South Sub County…… 57

Table 5.9: Radium equivalent ($Ra_{eq}$)……...……... 59

Table 5.10: Showing correlation of results of underground waters and sediments……61

Table 5.11: Radon activity in water samples for this work and various other regions……..……..……64

Table 5.12: Annual effective dose via ingestion of water for this work and various regions…….....64

## LIST OF FIGURES


Figure 1.1: Percentages for radiation doses from human-made and natural sources each year…….....2

Figure 2.1: Schematic diagram of the $\alpha$ - particle potential energy and daughter nucleus as a function of their separation…….……...….. 10

Figure 2.2: Relative predominance of the three main interaction mechanisms; photoelectric effect, pair production and Compton scattering ……..… 12

Figure 2.3: A Schematic diagram representing Compton scattering mechanism…… 13

Figure 2.4: A Schematic diagram showing a photoelectric interaction mechanism…….……... 14

Figure 2.5: A Schematic diagram Pair production mechanism…….....….. 15

Figure 4.1: Map of the Mutomo Sub County with sampled wells marked……..... 26

Figure 4.2: Block diagram of the solid-state detector ..... 30

Figure 5.1: Radon concentration in water in kBq/$m^3$ from a variety of both shallow wells and boreholes……. 41

Figure 5.2: Annual Effective Dose via ingestion of water from various water sources…….……..…. 44

Figure 5.3: Water to air dose distribution reported from various boreholes..... 45

Figure 5.4: Energy calibration fit used in this work..... 47

Figure 5.5: Efficiency response curve for the HPGe detector used.....49

Figure 5.6: Gaussian fit for $^{137}$Cs spectral peak at 661 keV ..... 50

Figure 5.7: Background corrected spectrum from a geogenic sample..... 52

Figure 5.8: Activity concentration of $^{226}$Ra, $^{232}$Th, and $^{40}$K in sediments sampled with water samples…….....…….. 54

Figure 5.9: Absorbed dose from sediments sampled from water points where the water samples were collected…….....……... 56

Figure 5.10: Annual effective dose rate reported from sediments sampled from various boreholes within Mutomo Sub County, Kitui County……. 58

Figure 5.11: Radium equivalent for sediments sampled from shallow wells and boreholes…… 60
Figure 5.12: Correlation between $^{226}Ra$ in sediments and $^{222}Rn$ in water from boreholes…….…….. 62
Figure 5.13: Correlation between $^{226}Ra$ in sediments and $^{222}Rn$ in water from shallow wells……..…….. .63

## LIST OF APPENDICES

Appendix i: Assembling RAD 7 Alpha detector in the field for Radon Measurements…… 75

Appendix ii: Water sample collection with the help of research assistant…… 76

Appendix iii: Research assistant siphoning water to collection bucket where vial is filled……77

Appendix iv: Local residents fetching tap water from water kiosk in Mutha Borehole……78

Appendix v: Researcher collecting water bulk water sample using bucket from a borehole in Mutomo area…… 79

## ABBREVIATIONS AND ACRONYMS

| | | |
|---|---|---|
| **AEDR** | **:** | Annual Effective Dose Rate |
| **CEMBS** | **:** | Central Eastern Mozambique Belt Segment |
| **DNA** | **:** | Deoxyribo Nucleic Acid |
| **EDXRF** | **:** | Energy Dispersive X-Ray Fluorescence |
| **US-EPA** | **:** | US-Environmental Protection Agency |
| **HPGE** | **:** | High Purity Germanium |
| **IAEA** | **:** | International Atomic Energy Agency |
| **GOK** | **:** | Government of Kenya |
| **LSC** | **:** | Liquid Scintillation Counter |
| **MCL** | **:** | Maximum Containment Level |
| **NaI (TI)** | **:** | Thallium Doped Sodium Iodide Detector |
| **NRC** | **:** | Nuclear Regulation Commission |
| **NCRP** | **:** | National Commission for Radiation Protection |
| **PIPS** | **:** | Passivated Implanted Planar Silicon Detector |
| **SGU** | **:** | Sweden Geological Survey |
| **SSI** | **:** | Swedish Radiation Protection Institute |
| **TAEC** | **:** | Tanzanian Atomic Energy Commission |
| **UNSCEAR** | **:** | United Nations Scientific Committee on Effects of Atomic Radiation |
| **ICRP** | **:** | International Commission on Radiological Protection |

## ABSTRACT

All living organisms continuously are exposed to natural radiation, which contributes most of the effective dose equivalent they receive. Radon, a naturally occurring colorless, tasteless and odorless radioactive gas is one of these radiations. The gas exists naturally in various environmental media such as water, geological sediments and air. It has gained focus since it is the largest contributor to radiation doses received by the human population via inhalation and ingestion posing great health risks. The main objective is to determine the radon levels in underground waters in Mutomo Sub County, in Kitui County using the RAD 7 alpha detector. The study further examined the radium levels in sediments collected from the proximity of sampled water sources using high purity germanium (HPGe) gamma-ray spectrometer to establish the correlation with radon in water. The radon concentration in water ranged from 0 - 120±6 $kBqm^{-3}$ with an average value of 30±1.5 $kBqm^{-3}$ which is above the recommended limit of 11 $kBqm^{-3}$ suggested by US-EPA, WHO and EU bodies. The calculated values for the absorbed dose are in the range 1.26 - 3.24 $mSvy^{-1}$, which is well below the recommended level. The annual effective dose (AED) via ingestion averaged 0.006±0.0003 $mSvy^{-1}$ while the radon in air from water averaged 0.07±0.003 $mSvy^{-1}$, which are both below the safety limit of 0.1 $mSvy^{-1}$ recommended by WHO 2004, and ICRP 2005 for ingestion and inhalation. Radium in sediments reported an average of 41±2.07 Bq/Kg which is above the world's average of 35 Bq/ kg reported in UNSCEAR reports. The radiation doses in water from sampled underground water are insignificant to term the water unsuitable for drinking and other domestic purposes. Correlational analyses between radium in sediments and radon in the water reported a weak positive coefficient suggesting a difference in the geological composition of surface matter and underground aquiver holding water.

# CHAPTER ONE

## 1.0 INTRODUCTION

### 1.1 Background to the Study

All living organisms are continuously exposed to radiation of natural origin, which contributes to most of the effective dose equivalent people receive. Radiations are both beneficial and harmful in case of long exposure to humans and the environment. Radiations are encountered in every day today life in various forms and intensities depending on the application and exposure duration (Halime *et al*., 2016). Natural sources of ionizing radiation include cosmic rays, gamma rays from geological materials, radon and its decay products in different media and various radionuclides found naturally in foods. 42% of natural radiation exposure originates from radioactive gas, radon. (UNSCEAR, 2008).

Radon is a colourless, tasteless and odourless gas, that exists naturally as three isotopes $^{219}$Rn (Actinon) from the $^{235}$U series; $^{220}$Rn (Thoron) from the $^{232}$Th series and $^{222}$Rn (radon) from $^{238}$U series. $^{219}$Rn and $^{220}$Rn exist in low concentrations because of their relatively short half-life (3.96 s and 55.6 s for $^{219}$Rn and $^{220}$Rn respectively). Radon $^{222}$Rn has a slightly longer half-life of 3.8 days. The relatively higher abundance of Radon-222 is usually attributed to the longer half-life of $^{238}$U (parent radionuclide whose half-life is $4.5 \times 10^9$years) which has not yet decayed to undetectable limits (UNSCEAR, 2000).

Radon gas escapes from the ground into the air, where it decays to daughter radioactive isotopes. The daughter radioactive products are either short-lived $^{218}$Po, $^{214}$Pb, $^{214}$Bi, $^{214}$Po or long-lived $^{210}$Pb, $^{210}$Bi, $^{210}$Po *(*Abu *et al., 1983).* Outdoors, radon is generally not a problem because it quickly diffuses to very low concentrations. However, indoor radon can accumulate to higher concentrations, especially in poorly ventilated dwellings. Indoor radon is, therefore, a product of different sources, which include construction materials, soil and water. Over 70% of the radon in water is usually released into the indoor air (WHO, 2009; Choubey *et al.,* 2005). Figure 1.1 shows contributions from various sources of radiation expressed as a percentage.

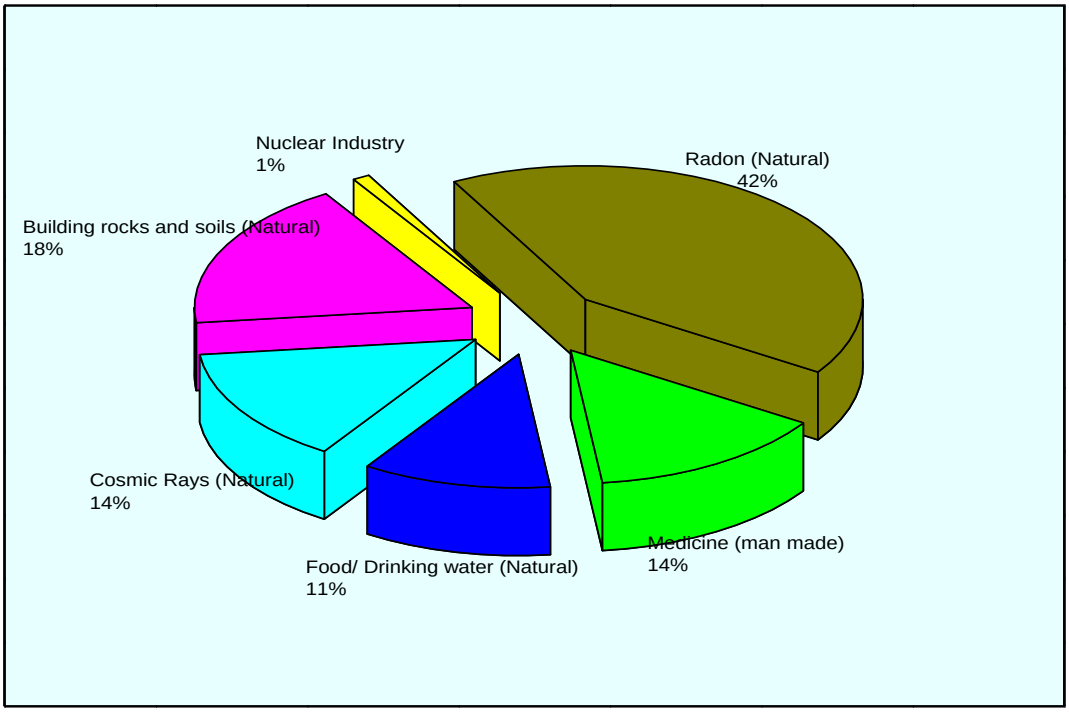


**Figure 1.1: Percentages for radiation doses from human-made and natural sources each year (UNSCEAR, 2000).**

Radon can enter the body through inhalation, food, and water consumption. The extent of radiation damage to the body depends on the exposed organ and the amount of dose received. The immediate effect of exposure to radon gas include cell and molecular modifications and in the long run stomach cancer, lung cancer or myoled leukemia have been reported depending on the pathway the potential radioisotope in water, food and inhalation gain entry into the biological system (Wanjala et al., 2021). Since water contributes significantly to indoor radon, *v*arious regulatory bodies around the world have given reference safety levels beyond which the water is termed contaminated by radon.

**Table 1.1: Reference levels for various Radon measurement parameters as outlined by various organizations**

| Parameter | Recommended level | Body |
|---|---|---|
| **Activity Concentration** | 200 - 600 $Bqm^{-3}$ | US-EPA, 1999 |
| | 100 $Bqm^{-3}$ or 11 $kBqm^{-3}$ | WHO 2004, EU 2001 |
| | 4 – 40 $BqL^{-1}$ | UNSCEAR, 2000 |
| | 11.1$BqL^{-1}$ or 300 pC $L^{-1}$ | ICRP, 2015 |
| **Annual effective dose** | 3-10 $mSvy^{-1}$ | US-EPA, 1999 |
| **(via ingestion)** | | WHO 2004, EU 2001 |
| **Annual effective dose** | 1 $mSvy^{-1}$ | ICRP 2005 |
| **(via inhalation)** | | |
| **World's Average** | 10 $BqL^{-1}$ | UNSCEAR, 2000 |

When radon levels in water surpass the reference level of 100 $Bqm^{-3}$ or the EPA's suggested upper limit for contamination (MCL)of 11.1 $BqL^{-1}$ the water is termed contaminated by radon. Population consuming such water may manifest harmful effects promptly or some years later depending on the amount of dose received by an individual. Radon, a decay product of the 238U series, delivers the biggest percentage of the total exposure, according to documented radiometric surveys. (UNSCEAR, 2000). This implies that the nature of underlying rocks will influence the radon levels in sub-surface water since the concentration of $^{238}U$ or $^{226}Ra$ in those rocks will eventually decay to radon.

Besides geology, other factors that affect the level of radon in water include; dilution of radon by rainwater, the temperature of the water more so for open waters, time of water flow for piped water due to desorption (Winde *et al.,* 2006). Due to the inconsistent supply of fresh water supply in Kitui County, many households depend on underground water from shallow wells whose information on the radioactivity level is unknown. This study aims at analyzing the radon levels in water from selected domestic shallow wells

and boreholes and seeks a correlation of $^{226}Ra$ in the sediments and $^{222}Ra$ in the wells studied.

## 1.2 Statement of the Problem

The rising population of Kitui county and particularly Mutomo Sub County has exerted a lot of pressure on existing water resources and forced residents to embrace alternative water sources to match the rising water demands. The larger population relies on the underground water from boreholes and shallow wells. The rocks in these water sources may have some minerals associated with high $^{226}Ra$, the immediate parent radionuclide of $^{222}Rn$. Radon being soluble in water can easily dissolve in water used for most domestic purposes including drinking and finding its pathway to the human biological system. Therefore, assessment of radon levels in water from shallow wells and boreholes in this area is critical in ascertaining the potential radiation exposure of residents from this pathway and the quality of water in general.

## 1.3 Objectives of the Study

### 1.3.1 Main Objective of the Study

To determine radon levels in underground water in Mutomo sub-county, Kitui County.

### 1.3.2 Specific Objectives of the Study

i. To determine the levels of radium ($^{226}Ra$) in sediments from boreholes and wells in Mutomo sub-county, Kitui County.
ii. To determine the levels of radon gas in underground water from Mutomo Sub County, Kitui County.
iii. To find out the correlation between $^{222}Rn$ in water and $^{226}Ra$ in Sediments.

## 1.4 Research Questions

i. What are the levels of radium $^{226}Ra$ in sediments from boreholes in Mutomo, Kitui County?

ii. What are the levels of radon gas in underground water in waters sampled in Mutomo, Kitui County?

iii. What is the correlation between $^{222}Rn$ in water and $^{226}Ra$ in sediments sampled from boreholes and wells in Mutomo Sub County, Kitui County?

### 1.5 Justification of the Study

Rapid population growth has increased the demand for safe water for domestic use. It is therefore important that the safety of this water is ascertained. Radon levels in water are very critical in safety analyses because the gas is radioactive yet it is odourless, tasteless and easily dissolves in water. Mutomo Sub County was chosen for the current study as a representative sub-county of Kitui because the fewer water sources available are within a blend of igneous, metamorphic and sedimentary rocks and support a larger population. Most shallow wells within the Mutomo area in the neighbourhood of peltic and semi-peltic rock systems, which has been associated with high mineralogy specifically ($^{232}Th$, $^{40}K$, and $^{238}U$) whose nuclides ($^{226}Ra$ and $^{222}Rn$) are soluble in water (Nugraha *et al.,* 2020). Besides, Radionuclides can also emanate from agricultural activities in the area.

In addition, since no other similar research has been carried out in the area, the findings from this study will be used as indicators of radon levels in water in this region. Further, recommendations from this study will be fundamental to policymakers, regulators, and the public. The data will also provide baseline information on the radon levels in water consumed in the area of study and add more information to the country's radiation mapping areas.

### 1.6 Scope and Delimitations of the Study

The study was conducted using water randomly sampled from boreholes in the Mutomo area in Kitui County. The study focused on the Mutomo area because most residents use water from shallow wells and boreholes for their domestic uses including drinking. The radon measurements were done in situ to ensure the quality of the data is maintained as radon may desorb and evaporate during transportation if the measurements were to be done ex-situ. The study focused on the assessment of the presence of $^{222}Rn$ radionuclides

in water from boreholes and establishing the current levels of $^{222}Rn$ levels in water used mostly in this area. Analysis of the water samples was conducted using Durrige RAD 7 Alpha detector from Water Resource Management Authority (WRMA) based in Kenya. The study further investigated the levels of radium from sediment samples sampled from shallow boreholes using a gamma-ray spectrometer at the Institute for Nuclear Science and Technology at the University of Nairobi.

# CHAPTER TWO

## 2.0 THEORETICAL CONSIDERATIONS

### 2.1 Radioactivity from Natural Sources

Radioactivity refers to spontaneous emissions of particulate or electromagnetic radiation from radionuclides whose atomic forces cannot keep the nucleus intact. Nuclear stability occurs when the ratio of proton to neutron is 1:1. Deviation from this ratio results in an unstable atom. Nuclear decay is through the emission of alpha, Beta and gamma rays. Alpha particle is equivalent to a Helium atom ($^{4}_{2}He$) and beta particle is equivalent to an electron ($^{0}_{-1}e$). From the theoretical aspect, a nucleus whose sum of the masses of its nucleons is less than the mass of the entire atom is termed unstable to beta and alpha decay. (Furusawa *et al.*, 2014).

Alpha or beta decay may leave the atom in an excited state. As the atom attains stability, it emits nuclear energy in the form of gamma radiation. The equation below shows the decay of the element ($^{A*}_{Z}X$) to ($^{A}_{Z}X$) which is accompanied by the emission of gamma radiation. Asterix indicates an unstable nuclide that decay by emitting radiation.

$$^{A*}_{Z}X \rightarrow {}^{A}_{Z}X + {}^{0}_{0}\gamma \quad \text{.....2.1}$$

There are two major sources of natural radioactivity; radionuclides of terrestrial origin and cosmic rays. Terrestrial radionuclides exist in crustal contents of different natures. Terrestrial radionuclides were trapped in rocks of different origins during the cooling of magma, which rocks resulted in the present rocks. Some rock species like igneous rocks are thought to have favoured the trapping of potassium radionuclide in its silicate bonds. Terrestrial radionuclides migrate in the ecosystem and exist in other media like water for the case of soluble minerals like potassium, radium and thoron gases. Particles encapsulated in dust particles may remain afloat in an air medium where they can be inhaled and access biological systems (Dodson, 1953).

Carbonitite rocks have high levels of radionuclides particularly thoron from ($^{232}$Th). A study done by Patel, 1991, Mustapha 1999 and Kebwaro 2011 reports high activity from primordial radioisotopes that were pegged to the abundance of rocks of igneous origin in the coastal strip.

**2.2 Activity of Radionuclides**

The activity (A) from the radioactive source is proportional to the number (N) of radionuclides present. Since the radioactivity intensity depends on the number of decaying radionuclides, it means that it decreases with time (Halliday, 1955). This further suggests that at the beginning of time, the levels of background radiation from terrestrial radionuclides posed higher radiation indices than the present. Equation 2.1 shows the rate of disintegration of a given nuclide at any time which is in direct proportion to the number of nuclei N of the nuclide present at that time.

$$-\frac{dN}{dt} \propto N \quad \text{.....2.2}$$

Where; the negative sign shows the diminution of the present number of radionuclides as the time *t* elapses.

$$-\frac{dN}{dt} = \lambda N \quad \text{.....2.3}$$

Where; λ is the radioactive decay constant, which is a constant of proportionality and it varies for each radioisotope.

If we set the boundary conditions; $N_0$ to be the undecayed nuclei at some time t, and at a later time the number to have decreased to *N*, which is given by the equation

$$N = N_0 e^{\lambda t} \quad \text{.....2.4}$$

The activity in the context of radioactivity refers to the absolute change in the number of nuclides with time i.e. $A = \left|\frac{dN}{dt}\right| = -\lambda N$. If we assume that when time t = 0 the activity = $A_0$, then the equation 2.4 can be rewritten as

$$A = A_0 e^{\lambda t} \quad \text{.....2.5}$$

The definition of Half-life ($t_{\frac{1}{2}}$)is the time taken for the number of active nuclei present in a source at a given time to fall to half its value (Cothern, 1987). It is given by the equation

$$t_{\frac{1}{2}} = \frac{0.693}{\lambda} \quad \text{.....2.6}$$

Where; Half-life $t_{1/2}$ and $\lambda$ is dependent on radionuclide instrumental in the identification of specific radionuclide.

**2.3 Theory of Alpha Emission**

Gamow *et al.,* 1928 developed the theory of alpha decay, which assumes that the alpha particle exists as a separate entity trapped inside the nucleus of the parent nuclide by a potential coulomb barrier. It follows that the system's potential energy varies as a function of distance, *r*, between their centres and for the alpha particle to liberate itself and escape from the nucleus; it must have sufficient energy to overcome the maximum potential energy barrier above its energy threshold of 4.2 MeV (Lilley *et al*., 2001).

Classically, such a particle would remain trapped inside the potential well barrier. However, the theoretical approach shows that there is a probability that the alpha particle can pass through the barrier and escape freely through the tunneling process shown in figure 2.1 (Kaplan, 1962). The potential barrier accounts for the fact that alpha particles emitted from heavy nuclei are supposed to exist within these nuclei for a short time before being emitted (Krane, 1988). The smaller the barrier width, the higher the probability that the alpha particle will be emitted and vice versa.

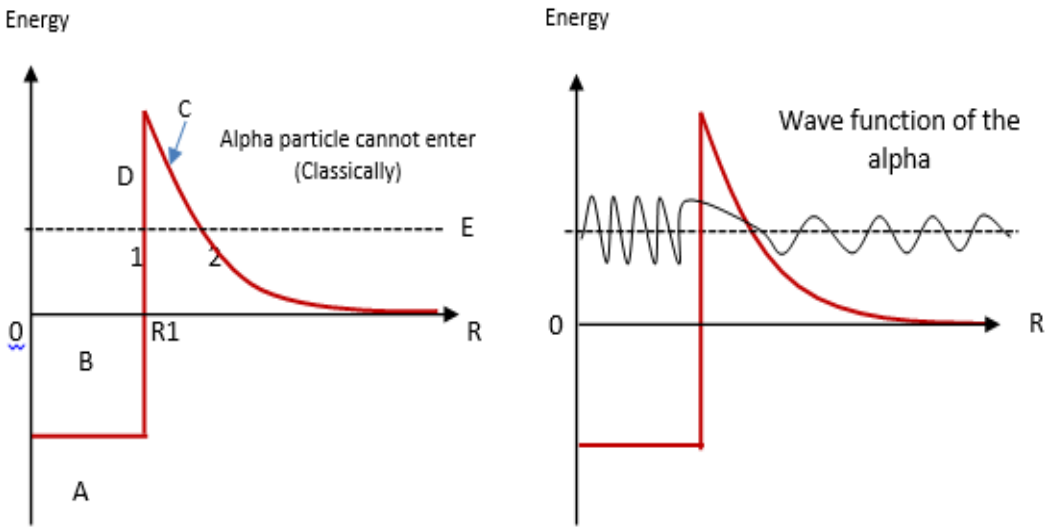


**A**-Attractive forces between nucleons particles **B**-Region where the alpha particle is trapped
**C**-Electrical repulsive forces within nucleus **D**-Energy barrier to be overcome
**E**-Energy of the Alpha particle emitted **1-2**-Potential barrier width

**Figure 2.1 Schematic diagram of the $\alpha$ - particle potential energy and daughter nucleus as a function of their separation (**Devaney, 1953**)**

Coulomb repulsion increases as r are decreased and increase sharply for the heavy nuclei because the disruptive Coulomb force increases with size at a faster rate as the square of the atomic (or proton) number $Z^2$ (force between nucleons). When the nuclei emit an alpha particle of higher energy, it might be left in the ground state, but when the alpha decay releases lower energy alpha particles, the latter is left in an excited state and acquire stability by the emission of electromagnetic gamma radiation or through internal conversion (Das *et al.*, 2003).

### 2.4 Alpha Interaction with Detector

There are two types of alpha particle detectors: those that use the energy spectrum of alpha particles to estimate radon activity, like the rad 7 alpha detector used in this study, and those that produce damage tracks when an alpha particle interacts with them, like solid-state nuclear track detectors do (SSNTD).

The RAD7 consists of a hemispheric chamber with a silicon alpha detector implanted in the middle that is lined with a conducting substance on the inside. In order to create an electric field across the volume of the cell, a high voltage in the range of 2000–2500V is supplied to the conductor in relation to the detector. A built-in pump with a variable flow rate is installed in the cell to enable drawing sample air through a hose. The hose has a filter installed to let gas through while preventing the passage of particle matter.The altered nuclei are driven towards the detector by the electric field as the isotopes decay inside the cell, where they adhere to the detector's surface. The progeny eventually decay, and the characteristic alpha radiation is released right into the silicon detector.

Because alpha particles are very ionizing, they interact with silicon chips to produce an electric current that is unique to alpha radiation. The isotope is then identified and measured using this. Every few hours, the detector must be flushed with dry, isotope-free air to remove the charged particles that have a tendency to collect on the detector surface over time.

Other detectors, such as the SSNTD, are covered in a substance called Polly allyl diglycol carbonate, which is a component of Columbia Resin (CR-39). At the site of contact, damage traces are left behind when alpha particles strike this layer of the detector. SSNTD, however, is unable to distinguish between the damage tracks caused by radon and thoron (Monnin et al., 1997).

The detector is contained in a container that slows down the entry of air containing the radon and thoron combination in order to achieve discrimination. The air takes longer to diffuse into the detector as a result of the slowing down, and because of the air's short thoron half-life (55.6 sec), it decays before reaching the alpha detecting chamber. Only radon, which has a half-life of 3.85 days, enters the detection chamber as a result. The alpha particles produced by the disintegration of the radon and its daughter are what are responsible for the subsequent damage tracks on the CR-39 alpha detector.

## 2.5 Radiation Interaction with Matter

Radiation interacts with matter through three main mechanisms; pair production, Compton scattering and photoelectric absorption. The probability of occurrence of each of these mechanisms is dependent on the energy of the photon. At lower energies, the dominant mechanism of interaction is photoelectric absorption, and at higher energies, pair production dominates. Compton scattering occurs for slightly higher energies than photo absorption. Figure 2.2 gives a summary of the interaction mechanisms at different energies and medium densities.

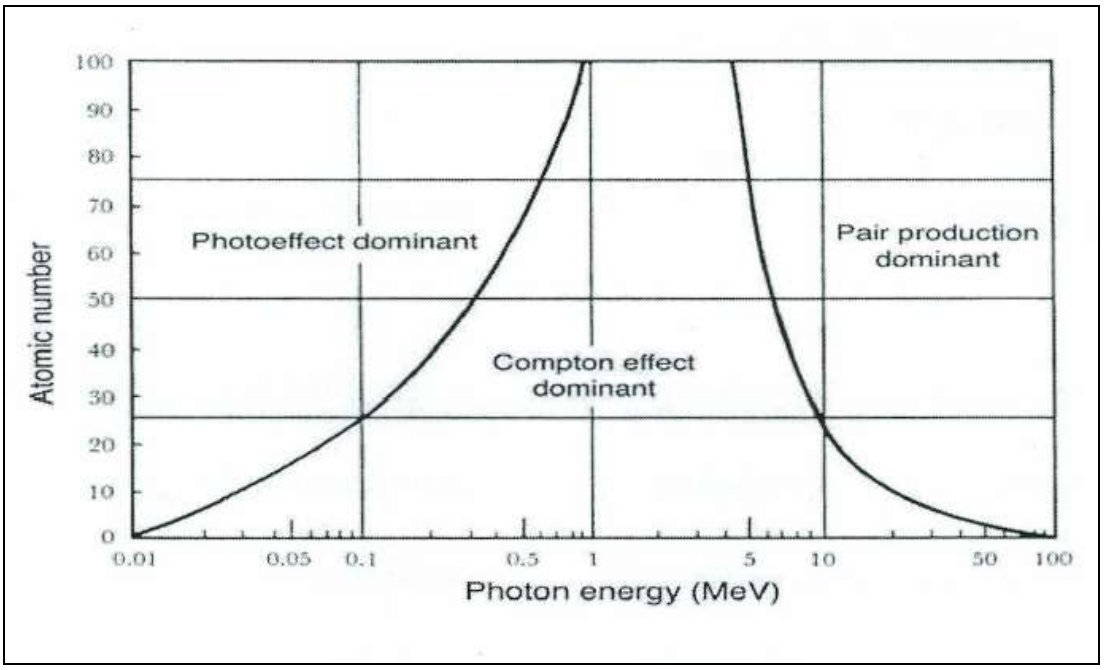


**Figure 2.2: Relative predominance of the three main interaction mechanisms; photoelectric effect, pair production and Compton scattering (Helmer, 1988).**

### 2.5.1 Compton Scattering

Interaction mechanism in which the incident photon transfers a fraction of its energy to an electron in the outer energy shells mostly outside K, L and M. The electron is assumed to be at rest (loosely bound). Depending on the energy of the incident photon, the position in the detector medium where the first interaction has occurred and the size and material of the detector, the scattered electron may not interact again. The energy

transferred to the electron is dependent on the angle at which the photon interacts with a stationary electron. The minimum energy transfer occurs when the θ=0. At θ=0, the photon transfers no energy to the detector and the incident photon retains its energy. The maximum energy occurs when θ=π. In this instance, the incident photon is backscattered and the stationary electron moves in the incident direction of the photon (Helmer *et al.*, 1988). A schematic figure showing Compton scattering is shown in figure 2.3

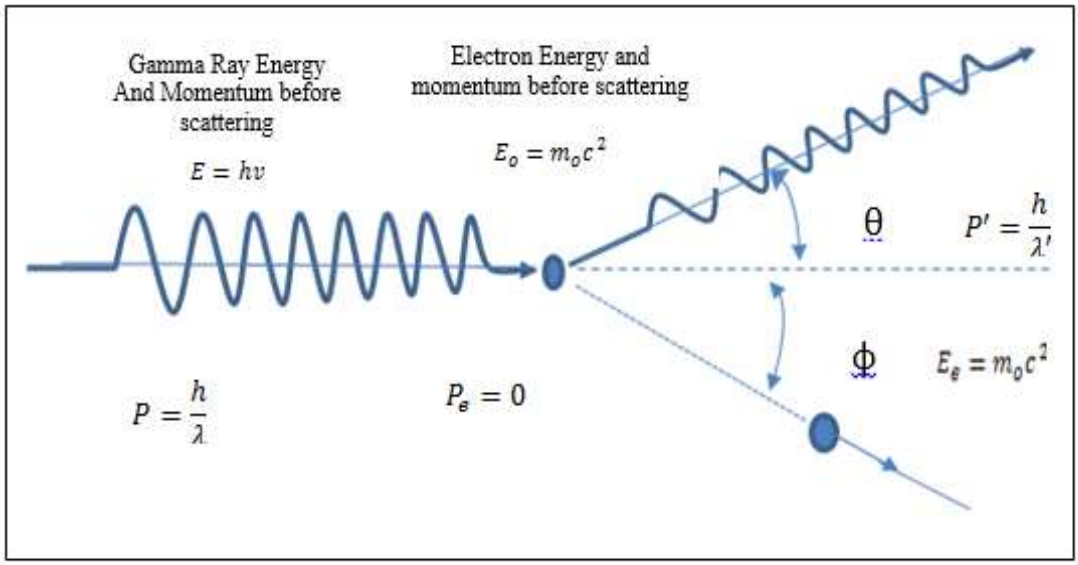


f

**Figure 2.3: A Schematic diagram representing Compton scattering mechanism (Helmer, 1988).**

### 2.5.2 Photoelectric Absorption

An incident photon interacts with an electron that is attached to one of the outer shells of an atom during photoelectric absorption. The photon is absorbed, causing an electron to be released from the shell that is most closely bound (the K-shell).photons with high energy are indicated by equation 2.9. The excited atom. Regains its equilibrium in two ways: by filling the void left by the An electron from a higher energy shell enters the photoelectron to fill it producing distinctive x-rays through the x-ray fluorescence technique) Figure 2.4a Photoelectric absorption may also result from the distinctive x-ray that is released. The Auger cascade is a method of spreading excitation energy among the remaining electrons that may result in the release of another electron as a means of

helping the atom regain equilibrium (figure 2.4 b). The freed photoelectron has kinetic energy that is equal to the difference between the incoming photon energy and the photoelectron binding energy in its original shell.

$$E_e = E_\gamma - E_b \quad \text{..... (2.9)}$$

Where $E_b$ is the electron's binding energy, $E_\gamma$ is the gamma-ray energy and $E_e$ is the photoelectron kinetic energy.

Figure 2.4 is a diagram showing a photoelectron interaction mechanism

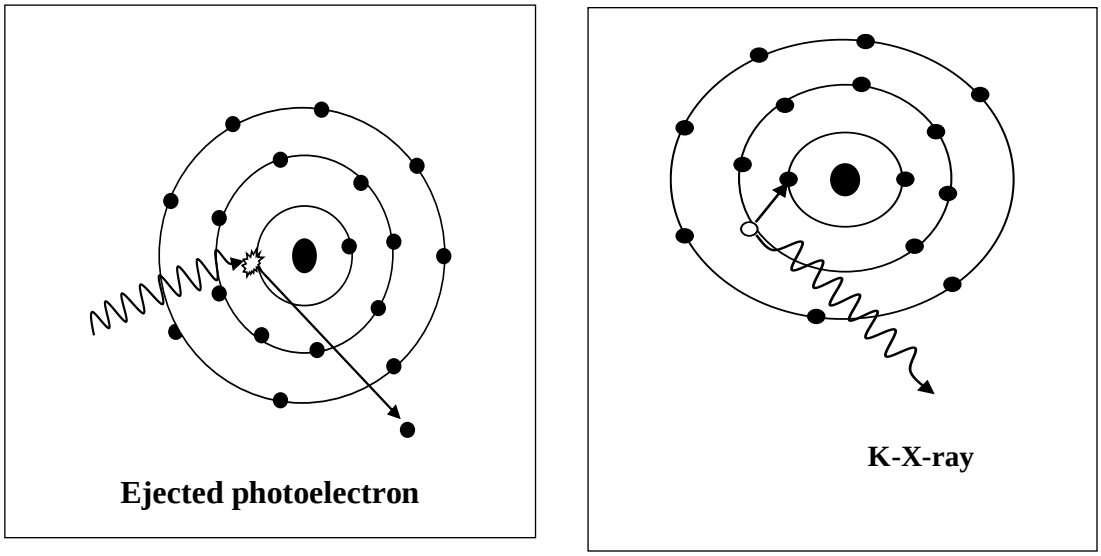


**Figure 2.4: A schematic diagram showing a photoelectric interaction mechanism (Helmer, 1988).**

### 2.5.3 Pair Production

To maintain momentum, pair creation is the direct conversion of the photon's burst of electromagnetic energy into the production of an electron and a positron close to the nucleus. The incident gamma ray energy must be more than the electron's twice resting mass energy of 1022 MeV for it to happen (Hall *et al.*, 2011) within the powerful electric field of the nucleus, the gamma-ray photon vanishes, producing an electron-positron pair (IAEA, 2005). The incident energy hv, or hv 2m c2 e, is transformed into the motion of the electron-positron pair at energies above 1.02 MeV. The extra energy is shared

symmetrically and asymmetrically between the electron-positron pair at low energies E 50MeV g and high energies E is greater than 1GeV g.

The following equation demonstrates how the discrete quantum energy is distributed among the latter.

$$E_e = E_\gamma - 1022 \quad \text{.....2.10}$$

Figure 2.5 summarizes the pair production mechanism with incident photon producing two particles oppositely charged.

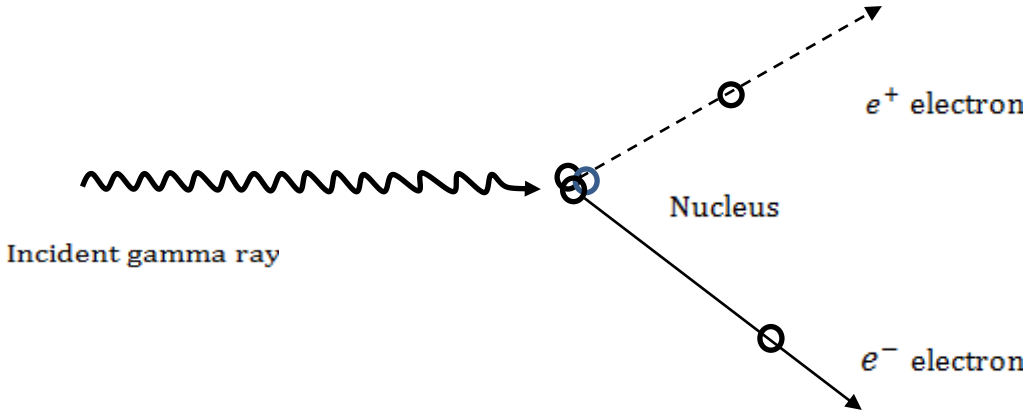


**Figure 2.5: A Schematic diagram Pair production mechanism (Helmer, 1988)**

### 2.6 Radioactive equilibrium

Radioactive equilibrium refers to relativity in the activity of the radionuclide and its decay daughters in a decay progression. Some forms of equilibriums like secular are used in the calculation of the activity from a certain decay chain relying on the activity of short-lived radionuclides. Some forms of equilibriums include transient and non-equilibrium, which are discussed below. Non-equilibrium occurs when the half-life of the daughter nuclide is greater than that of the parent and thus the activity of the parent vanishes leaving behind the daughter nuclide (Gilmore, 2008). The following conditions must hold;

$\lambda_d < \lambda_p$ Or $(t_{1/2})_p < (t_{1/2})_d$. Such a condition occurs in the transmutation of $^{218}$Po ($t_{1/2}$= 3.10 minutes) to $^{214}$Pb ($t_{1/2}$= 26.8 minutes).

Transient equilibrium occurs when the half-life of the parent is long compared to the half-life of the daughter. This means if a sample is sealed and left undisturbed when the activity of the daughter nucleus builds from zero to a maximum value and decays apparently with the same half-life as the parent nuclei. (Gilmore, 2008). An example of this equilibrium occurs for the transition of $^{212}$Pb ($t_{1/2}$ = 10.64 hours) to $^{212}$Bi ($t_{1/2}$ = 60.55 minutes) from the thorium series since $\lambda_p < \lambda_d$ or $(t_{1/2})_d < (t_{1/2})_p$.

The total activity in the sample is the sum of the parent and daughter's activities. When the daughter radionuclide transforms at the same rate as it is being formed, and its total activity then decays at the same rate (at t = ∞) as the original parent nuclide, the two species of decaying nuclei are termed to be in transient equilibrium.

Secular equilibrium is established on the condition that the daughter and the parent radionuclide are sealed together and further that the half-life of the parent radionuclide is very long compared to that of the daughter progeny. Since the half-life of the parent radionuclide is very long such that it does not decay notably compared to the daughter nuclide, the level of the activity of the daughter accumulates such that it decays at the same rate at which it is being formed. In this instance, the activity of each progeny equals that of the parent radionuclide. The total activity is n times the original activity of the original parent radionuclide.

Secular equilibrium occurs in the thoron and radon decay series. The transitions of $^{238}$U→$^{234}$Th→$^{234}$Pa in the Uranium decay series and $^{232}$Th→$^{228}$Ra→$^{228}$Ac in thorium decay progression. In each of the above scenarios, the half-life of the parent radionuclide is greater than that of the daughter, thus the establishment of secular equilibrium between each pair is possible. The activity of $^{234}$Th and $^{234}$Pa + $^{234}$Pa will be equal to that of $^{238}$U and the activity of $^{228}$Ra and $^{228}$Ac will be equal to that of $^{232}$Th. The total activity will be three times that of the $^{238}$U and $^{232}$Th, respectively. Thus if the activity of one of the

radionuclides in a decay chain can be measured, it can be assigned to the other radionuclides within the chain, i.e. assuming equilibrium.

# CHAPTER THREE

## 3.0 LITERATURE REVIEW

### 3.1 Introduction

This chapter examines related research carried out in different regions of the world.

### 3.2 Surveys on Radon outside Kenya

Aruwa *et al.,* 2017, evaluated $^{222}Rn$ levels in groundwater from wells and boreholes in Idah, Kogi state in Nigeria. The study used a Liquid Scintillation Counter (LSC) for data collection. The radon analyses report an average concentration of 13.45±1.00 $BqL^{-1}$ for waters from wells and 14.09±1.10 $BqL^{-1}$ for borehole water. The research attributed higher radon in borehole waters to depth as bedrock waters have radon due to higher radium in the underground waters. The overall mean radon concentration recorded was 13.77±1.05 $BqL^{-1}$. The findings compared well with data from other similar surveys and they were in a reasonable range with a Maximum Contamination Level of 11.1 $BqL^{-1}$ suggested by USEPA and slightly above the world's average of 10.0 $BqL^{-1}$ for drinking water. The reported annual average dose via ingestion was 0.049 and 0.051 $mSvy^{-1}$ for well and borehole waters respectively. The AED for borehole and well waters was far below 3 - 10 $mSvy^{-1}$ the recommended intervention range by ICRP. The study concluded that the use of water from the surveyed wells and boreholes had an insignificant threat to those who use this water for drinking purposes.

Sudhir *et al.,* 2016, analyzed radon concentration in 20 water samples from various locations of the Rajasthan district in North-West India. The study-detected ∝-particles from emissions of $^{214}Po$ and $^{218}Po$, which were done using RAD $H_2O$ accessory connected to RAD 7 electronic alpha detector. The radiometric survey reported radon concentration in the range of 0.50 - 22 Bq $l^{-1}$ with an average of 4.42 Bq $l^{-1}$. The mean value lies within the safe limit of 4-40 Bq $l^{-1}$ (USCEAR 2008). The Average Effective Dose ranged from 1.37 to 60.06 $\mu Sv/y^{-1}$ which is far below the safe limit of 0.1 mSv $y^{-1}$ (WHO 2004, EU 1998). The study concluded that consumption of water from the

surveyed water points presents no significant radiological threat to the inhabitants of the area.

Nasir *et al.,* 2012 analyzed Radon levels in 20 samples collected from ponds, wells and Taps in Kulachi city of Pakistan. (Columbia Resin-39) based NRPB (National Radiological Protection Board) radon dosimeters were used to measure the radon concentration. Radon concentration calculated from etching the track densities using 6M NaOH solution ranged from 1.218 ± 0.005 $BqL^{-1}$ from tap water to 0.602 ± 0.003 $Bql^{-1}$ in tap water. High radon levels in well water were attributed to depth as most of the well waters are 150 feet in depth and bedrock water from consistent surveys has reported elevated concentrations of radon isotope. The AED evaluated varied from 4.39 × $10^{-3}$ $mSvy^{-1}$ to 8.89 × 10-3 $mSvy^{-1}$. The upper level of radon concentration as well as AED was within the US-EPA and WHO recommended limits.

Ali *et al*., 2010, used RAD-7 to analyze 55 water samples from various boreholes and shallow wells in Islamabad in Pakistan. The area terrain is hilly and relatively rocky with Siltstone and Sandstones dominating the geology of the Muree area. The study reports an average of 88.63 $kBqm^{-3}$ with a range of radon concentrations in water of 25.90 - 158.40 $kBqm^{-3}$. The average annual effective dose reported is 2.023 $mSvy^{-1}$ which was within the recommended levels. Ahmed *et al.,* 2004 analyzed groundwater from wells in Egypt for $^{226}Ra$ and $^{232}Th$ using Alpha Spectrometer RAD7 Detector. The study compared results with that of tap water. Although the content of the radionuclides was found to be within acceptable limits, higher values were reported in groundwater than in tap water.

Nwankwo *et al.,* 2013 carried out a study on the estimation of $^{226}Ra$ and $^{228}Ra$ concentrations in water samples from groundwater sampled from Tanke-Ilorin, Nigeria. Ten water samples were subjected to analysis using the gamma-ray spectrometry technique to establish the specific levels of $^{226}Ra$ and $^{228}Ra$. The findings reported mean activity ranging from 0.81 ± 0.08 to 7.4 ± 2.2 Bq/l for $^{226}Ra$ and 1.8 ± 0.3 to 5.6 ± 2.6 Bq/l for $^{228}Ra$. The estimated AEDR received by the population through ingestion of

$^{226}$Ra ranged from 0.81 to 1.74 mSv/y with an average of 1.30 mSv/y. The average contributions from the activities of both $^{228}$Ra and $^{226}$Ra reported by this study were higher than the world's admissible level of 1 mSv/y suggested for the general public by ICRP and 0.1 mSv/y by WHO reports.

Thabayneh *et al.,* 2012 evaluated natural radioactivity concentrations and their associated AEDR in 60 water samples randomly collected from Hebron province, West Bank, Palestine using High purity germanium spectrometry. The activity concentration reported a range of 1.62 to 9.11 Bql$^{-1}$, 0.45 to 4.40 Bql $^{-1}$, 0.44 to 2.06 Bql$^{-1}$, and 1.57 to 15.60 Bql$^{-1}$ for $^{226}$Ra, $^{232}$Th, $^{234}$Th, and $^{40}$K, respectively. The dose to the adult population through ingestion of water was estimated by evaluating the effective dose that averaged 0.56 mSvy$^{-1}$ for $^{226}$Ra, 0.04 mSvy-1 for $^{40}$K, 0.065 mSvy-1 for $^{232}$Th, and 0.042 mSvy$^{-1}$ for $^{234}$Th. Some sampled sites reported doses above the recommended annual effective dose.

### 3.3 Radon Surveys in Kenya

Mustapha *et al.,* 2002 carried out a screening survey to evaluate the levels of radon in water used for drinking in various locations in Kenya. The study reported a maximum value of 410 Bq L$^{-1}$ with an average value of 37 Bq L$^{-1}$. The lithology of the surveyed locations in Kenya lies within three systems of geology; Sedimentary, Precambrian and Volcanic systems. Some of the water sources surveyed include piped treated water, springs and shallow wells. Generally, the groundwater sources reported enhanced levels of $^{222}$Rn as compared to surface waters. A strong correlation is noted between the radon level and geological blueprint. High radon levels in the water were reported from water sources under lied by rocks enriched with $^{222}$Rn precursors like volcanic and granitic species. Similarly, a lower concentration of radon radioisotopes was reported in predominantly sedimentary areas. The survey recommended no remedial action at the time of the survey. Nevertheless, some homes reported indoor radon exposures and radon levels above the recommended level.

Chege *et al.*, 2004 did a survey on Thoron emanation and exhalation in Mrima hills using various samples among them cassava tubers, building materials, water samples, air and sediments. A couple of detectors including an accumulation chamber coupled with a RAD7 monitor for exhalation measurements, HPGe detectors and CR-39 SSNTD was instrumental for simultaneous measurements of $^{222}$Rn and $^{220}$Rn. HPGe detector was useful for the determination of radioactivity measurements in crops and water samples. Gamma-ray spectrometer reported an average activity concentration in building materials averaging 134 Bq kg$^{-1}$ and 431 Bq kg$^{-1}$ for $^{226}$Ra and $^{232}$Th respectively.

Chege et *al.*, 2014 analyzed groundwater sampled from Mrima hills and Kanana village in south coast Kenya. The study aimed at determining the levels of $^{226}$Ra, $^{232}$Th and $^{40}$K in water. Kanana water samples had an undetectable level of $^{226}$Ra of less than 5 Bq kg$^{-1}$. The maximum $^{226}$Ra level reported was 13.2±1.2 Bq l$^{-1}$ with 37% of total water samples from Mrima hills having $^{226}$Ra exceeding the acceptable level of 1Bq l$^{-1}$. Due to the partial solubility of $^{226}$Ra, its presence suggested it could be abundant in the local geology. The maximum value of the Annual effective dose reported by this work was 3.3 mSv/y$^{-1}$ with an average of 1.7 mSv/y$^{-1}$ which exceeded the WHO dose limit of 0.1mSv/y$^{-1}$ via ingestion which is equivalent to 10 % of the total exposure of 1 mSv/y recommended by ICRP for the general public. The effective dose due to groundwater consumption exceeded ICRP's prescribed limit and remediation measures were recommended.

### 3.4 Natural Radioactivity of Sediments

Faanu *et al.*, 2016 did a survey on in-situ radioactivity using environmental samples; soil, ore samples and rocks, from Perseus Ghana established. The mean radium concentration at a 1 m radius round center was done for each sampling point to ensure that the representation of the sample was improved thus a mean of 257 Bq/Kg with a range of 136.6–340.2 Bqkg$^{-1}$. The external and internal indices averaged 0.7 ± 0.2 and 0.9 ± 0.2 respectively. The total AEDR from the sediments evaluated in this study averaged 0.918 mSv. The findings on the levels of ambient radiation compare well with similar studies

available in the literature and the extreme values are within the safety levels suggested in ICRP reports of 1 $mSvy^{-1}$.

Mustapha *et al.*, 2002 experimented on exposing radiation from various components among them water, ore and dust in Mrima Area. The spectrometric analyses of the radioactive component in drinking water report a range of 1 to 410 Bq/l. The study was carried out using a conventional liquid scintillator. Roughly 155 water samples were collected using 20 ml glass vials for analysis from various water sources; rivers within the locality of Mrima hills treated piped water from the municipality, streams and shallow wells.

Wanjala *et al.,* 2015 studied the elemental concentration in the rocks and soils around Ortum. Radioactivity measurements in the field were determined using the handheld RedEye and Radiagem radiation survey meters. High Pure Germanium (HPGe) detector was adopted in the quantitative evaluation of the levels of naturally occurring radionuclide Uranium-238 ($^{238}U$), Thorium- 232 ($^{232}Th$) and Potassium-40 ($^{40}K$) in the soil and rocks. Liquid Scintillation Counter (LSC) was useful for the analysis of water samples while the Energy Dispersive X-Ray Fluorescence Spectrometer (EDXRF) was used to determine the elemental composition in the rocks and soil. The RESidual RADioactivity (RESRAD) program analyzed the spectral data to assess the doses and risks, which may emanate from the radiation exposure in the Ortum region.

Herman *et al.,* 2019 surveyed the elemental and radioactivity measurements in Minjingu mining located in the Northern part of Tanzania since it was known for high natural background radiations that were mainly associated with geological contributions from several phosphate deposits that are explored for exportation and industrial manufacture of fertilizers. It was determined using Energy Dispersive X-ray Fluorescence while the outdoor dose rate and the activity levels of samples from around the mine were determined using a gamma spectrometer system with a Hyper Pure germanium detector system. The activity concentration for the $^{238}U$, $^{228}Th$ and $^{40}K$ radionuclides revealed

activities ranging between 49±1 Bqkg$^{-1}$ to 241±6 Bqkg$^{-1}$, 51±2 Bqkg$^{-1}$ to 211±5- Bqkg$^{-1}$ and 666±29 Bqkg$^{-1}$ to 1076±45 Bqkg$^{-1}$ for$^{238}$U, $^{228}$Th and $^{40}$K respectively. These values exceeded the limit average activity concentration of 40 Bqkg$^{-1}$, 35 Bqkg$^{-1}$ and 420 Bqkg$^{-1}$ for $^{238}$U, $^{228}$Th and $^{40}$K relative to the selected research sites. The dose received by the population around Minjingu was 147±3 nGyh$^{-1}$which is almost three times the average limit of 50 nGyh$^{-1}$. The findings suggested radiation health risk to the population and therefore realistic quantification of the overall exposure of workers and public at Minjingu, and remedial measures for future radiation safety to be taken.

Mutungi *et al.,* 2018 carried out a survey on the evaluation of the levels of natural radioactivity in the geological samples obtained in Makueni County using the gamma-ray spectroscopy method. The study's soil samples had average concentrations of 238U, 232Th, and 40K of 69 + 5 BqKg-1, 53 + 3 BqKg-1, and 1098 + 69 BqKg-1, respectively, whereas the activity concentrations of the rocks were 139 + 6 BqKg-1, 73 + 3 BqKg-1, and 1573 + 65BqKg-1, respectively. In general, activity concentrations in rocks and soils were found to be 104 + 5 BqKg-1, 63 + 3 BqKg-1, and 1336 + 67 BqKg-1 for 238U, 232Th, and 40K, respectively, above the world average values. However, it was shown that the doses were higher than the global average of 60 nGyh-1 (UNSCEAR, 2002). Estimates of the effective dose rates for human exposure to 238U, 232Th, and 40K ionizing radiation in soil samples were determined to be 0.29 + 0.02 mSvy-1 and 0.45 + 0.02 mSvy-1, respectively. Health hazard values were below the safety level of 1.0 mSvy-1 (ICRP, 1991; UNSCEAR, 2002), hence residents of the chosen location were not at substantial risk of health problems. He advised the government and non-governmental organizations to use this study as a baseline investigation on the levels of radioactivity in the area because the building materials from the studied area were safe for use.

Elijah *et al.,* 2016 did analysis of soil samples from wheat plantations in Narok County, Kenya using a NaI (TI) gamma-ray spectrometer, From soil samples, it was possible to estimate the quantities of 238U, 232Th, and 40K specific activities. It was determined that the mean values for 238U, 232Th, and 40K were above the global average since they

were 52.34.2 Bqkg-1, 61.33.9 Bqkg-1, and 1383.649.1 Bqkg-1, respectively. Further calculated radiological health hazard indices using conventional analytical methods revealed a mean value of 246.59.6 Bqkg-1 of radium equivalent, while the corresponding values for absorbed dose rate (DR) and annual effective dose equivalent (HR) were 122.49.6 nGyh-1 and 0.600.03 mSvy-1, respectively. The values for the gamma and alpha indices were 0.94 and 0.03 and 0.26 and 0.02 respectively, whereas the external and internal health hazard indices were 0.66 and 0.03 and 0.81 and 0.04 respectively. The United Nations Scientific Committee on the Effect of Atomic Radiation (UNSCEAR, 2002) results for this environment for radiation hazard indices were lower than those values in the world. The study characterized the risk brought on by radiation exposure in the Narok County wheat cultivation region as negligible.

Determination of radium concentration from soil samples collected from wells where the water samples were collected is of great importance. This is because studies show a great correlation between the mineralogy of rocks and that of water. The contamination may occur because water from deep wells oozes from rock grains and soluble elements dissolve in it. Evaluation of radionuclides in water was necessary for the quality control of data. Extremely high Radionuclides (radium) contents in the soils and rocks will suggest a possibility of corresponding high radon levels in the water. From the literature review, it is evident that Radon poses a health hazard to human beings and its presence in the underground waters therefore their levels differ with the geology of the area. In addition, very few studies related to radon have been done in Kenya. Motivated by this, The present study was carried in. the Mutomo area in Kitui County.

# CHAPTER FOUR

## 4.0 MATERIALS AND METHODS

### 4.1 Study Area

The research was carried out in the Mutomo area, the southern part of Kitui County, Kenya spanning an area of 12,496.40 $km^2$ with an approximate population of 113,356 according to the 2019 population census (KNBS, 2019). Mutomo town is approximately 70 km from Kitui County headquarters and 230 km from Nairobi. It lies on Latitude $1^0$45'0" S to$1^0$54'0" S and Longitude $38^0$ 18'$^0$" E to $38^0$28" E and 696 m above sea level. Mutomo is a semi-arid area that receives little rainfall showers around the year making it harsh weather conditions.

The lithological units in the Mutomo area are placed into three categories: Archean rocks of the Basement System, Tertiary Yatta Plateau system and the superficial deposits of Pleistocene to Recent age which manifest different variations in levels of radon concentrations (Dodson 1953). To the east of Mutomo town is an expansive Kanziko limestone deposit. The water sources include protected and unprotected shallow wells, seasonal rivers and man-made boreholes. A larger population relies on surface water from shallow wells. However, a treated piped water system is available but not sufficient to address the water needs of the population more so in densely populated towns. Figure 4.1 shows the points, which were sampled for the water and radium. The points show a uniform spread of the water points in the studied area.

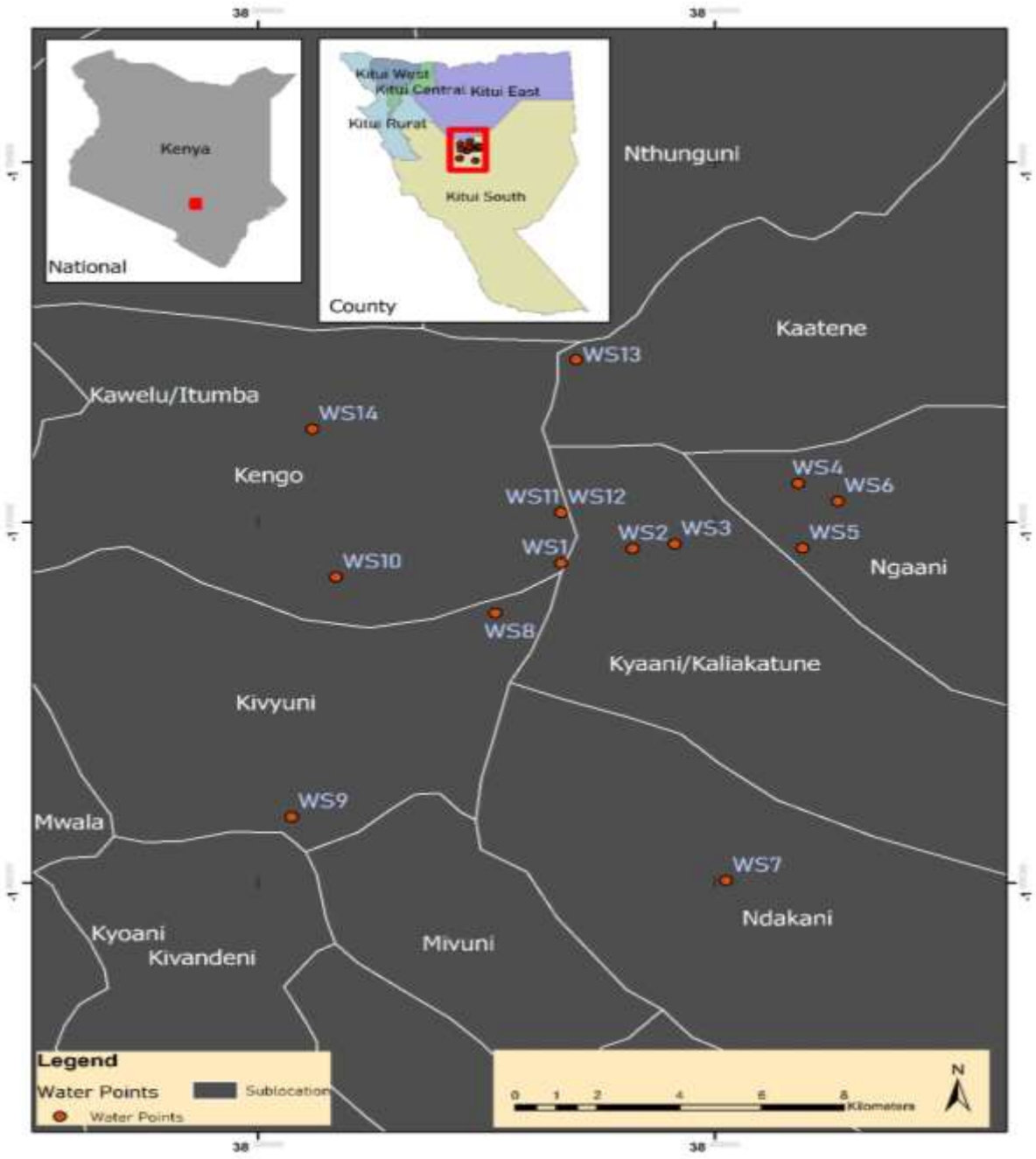


**Figure 4.1: Map of the Mutomo Sub County with sampled wells marked**

**Table 4.1 shows a summary of sampled GPS locations and elevations**

| S/no | Sample ID | Geo- Reference | Elevations |
|---|---|---|---|
| 1 | Munyoki A | 38.37S:1.81E | 653.7 m |
| 2 | Kasiluni | 38.38S:1.80E | 648.9 m |
| 3 | Kavuse | 38.39S:1.80E | 664.7 m |
| 4 | Ngosini | 38.41S:1.79E | 720.0 m |
| 5 | Mutha town | 38.42S:1.80E | 640.1 m |
| 6 | Kawambemba | 38.42S:1.79E | 646.9 m |
| 7 | Yimikoongoo | 38.35S:1.82E | 688.2 m |
| 8 | Katuuni | 38.30S:1.88E | 837.3 m |
| 9 | Musila | 38.31S:1.81E | 650.4 m |
| 10 | Kyanga | 38.36S:1.79E | 521.9 m |
| 11 | Makutano | 38.36S:1.75E | 541.9 m |
| 12 | Muliluni | 38.38S:1.80E | 640.8 m |
| 13 | Kwa Nzalu | 38.40S:1.79E | 720.3 m |
| 14 | Munyoki B | 38.37S:1.80E | 660.2 m |
| 15 | Kwithima | 38.31S:1.77E | 619.0 m |

### 4.2 Materials used in Measurement of Radon in Water

The following materials were used in the collection and measurements of radon levels in sampled water. Android Mobile Phone with GPS and Map Essentials application for identification of the geographical positions of the sampled boreholes. A 10-litre bucket for provisional collection of water from the wells, 250 ml vials with tight-fitting cork for holding 250 ml of the water sample, RAD $H_2O$ accessory connected to RAD 7 detector for detection and quantification of alpha from which radon levels were estimated, and water samples from the various surface and underground sources.

### 4.3 Collection of Water Samples

Water samples were collected from three categories of water sources namely; springs boreholes and wells. Systematic random sampling was used during water sampling from

wells and boreholes near Mutomo town as they supply water for drinking to a larger population compared to those in the outskirts. From each division, at least three water samples from various shallow wells and boreholes were collected. Fifteen (15) water samples from the most relied-on water points were collected. These samples were statistically sufficient to represent the surveyed area fully. The water was siphoned from the well using a long pipe until its flow was steady to ensure that no air bubbles along the lining of the pipe. The water was then tapped into a bucket of approximately 10 litres until it overflowed. A glass bottle was first rinsed using the water to be sampled to ensure traces of water from the previous sample were not mixed with the other samples collected. The 250 ml vial was submerged gently and vertically into the water in a bucket and tilted to ensure that all the air bubbles escape. The bottle was maintained underwater until it filled.

While the vial is still submerged, the cap of the vial was screwed and ensured that the sample contained no bubble or headspace this procedure was repeated for all water samples. Water sampling was done in the morning and the evening hours when the temperatures were low to ensure the water has a high concentration of dissolved radon gas. Since during midday, the temperatures are high and the dissolved radon gas escapes into the environment leaving a low concentration, which might affect the quantitative aspect of the data.

### 4.4 RAD 7 Alpha Detector

It is a precise radon and thoron detector used in radiation detection and monitoring for both laboratory and in-situ measurements. It is a versatile and affordable radiation detector. Rad-7 detector has silicon that is used as a semiconductor material for converting alpha radiation to electrical energy. It is useful for measuring radon concentration in waters, soil and indoors. It is a portable spectrometer caged in a rugged case to ensure its safety when in transit. The Rad 7 detector has a detector inside it that distinguishes alpha $^{214}$Po and $^{218}$Po with a range of energy of 7.9Mev and 6.0Mev respectively.

It consists of the following components; a detachable wireless printer, a built-in air pump with rechargeable batteries and a preinstalled DURRIGE software for analyses and statistical graphing. The RAD7 can acquire and store large amounts of data on radon and thoron for later offline printing.

### 4.5 RAD 7 Detector Characterizations

RAD7 alpha detector is a detector for detecting radon using alpha energy spectrum emitted during bubbling process. A high voltage in the range of 2000 - 2500 V is applied to the conductor relative to the detector hence creating an electric field throughout the volume of the cell.

The cell is equipped with a built-in pump with an adjustable flow rate to allow drawing sample air through a hose. The hose is fitted with a filter to allow the gas to pass through while blocking the entry of the particulate progeny.

The altered nuclei are driven towards the detector by the electric field as the isotopes decay inside the cell, where they adhere to the detector's surface. The progeny eventually decay, and the characteristic alpha radiation is released right into the silicon detector. Alpha particles are extremely ionizing, and when they contact with silicon, they produce an electric current that is distinctive to alpha radiation and is used to identify and measure the isotope. Every few hours, the detector must be flushed with dry, isotope-free air to remove the charged particles that have a tendency to collect on the detector surface over time.

Rad 7 was preferred over SSNTD due to its ability to discriminate, and damage tracks from radon and thoron. The detector precisely distinguishes alpha $^{214}$Po and $^{218}$Po within a range of energy of 7.9Mev and 6.0Mev respectively.

This is achieved by enclosing a detector in a container that slows down the entry of air containing the mixture of radon and thoron.

Slowing the air entry increases the diffusion length of the air and short-lived thoron (half-life 55.6 sec) decays before entering into the alpha detecting chamber. Consequently, only radon (half-life 3.85 days) proceeds to the detection chamber. The resulting damage tracks on the CR-39 alpha detector are attributed to alpha particles from the radon and its daughter's decay. Figure 4.1 summarizes the structural components of the RAD 7 detector.

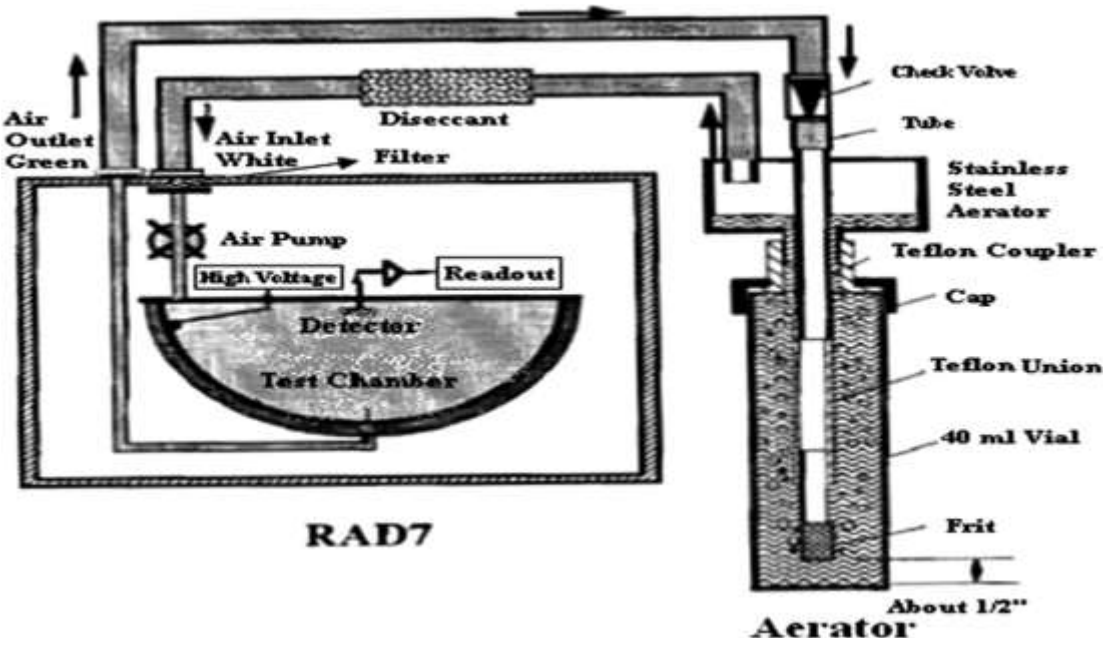


**Figure 4.2: Block diagram of the solid-state detector (Rani *et al.*, 2013)**

### 4.6 Radon Measurement using RAD 7 Detector

A bottle holding 250 ml of water was connected to RAD-7 and the internal air pump of the radon monitor was put on for re-circulating a closed air loop through the water sample, purging radon from the water into the air loop. The air was recirculated through the water continuously to extract the radon until the RAD $H_2O$ system reached a state of equilibrium within 5 min, after which no more radon could be extracted from the water. After attaining equilibrium between water, air, and radon progeny attached to the passivity implanted planar silicon detector.

The RAD-7 detects the alpha decaying radon progenies from $^{218}Po$ and $^{214}Po$ using passivated implanted planar silicon detector. The radon monitor (RAD-7) uses a high electric field above a silicon semiconductor detected at ground potential to attract the positively charged polonium daughters $^{218}Po$ and $^{214}Po$ which are counted as a measure of Radon-222 concentration in air. The radon activity concentration measured in the air loop was used for calculating the initial radon-in-water concentration for the respective sample. The RAD 7 detector gives a report on a print out showing the average radon readings from the four cycles which were averaged to increase the data reliability and quality by minimizing errors. Each sample was analyzed at an interval of 5 minutes, which is assumed as the time the radon gas attains equilibrium with its decay daughters. The process was repeated for at least 4 cycles before printing out for a good average. This process took 30 minutes per sample. The mean concentration for each sample represented the radon activity in water samples from a selected well or borehole. The activity values were calculated at a confidence level of over 95% which assures data quality. Other dose parameters like AED and absorbed dose were evaluated from radon activity.

### 4.7 Radon Analysis

#### 4.7.1 Radon Activity Concentration (Bq $m^{-3}$)

Radon measurements were estimated using the RAD 7 alpha detector which uses mathematical equation 4.1 to estimate the radon activity in the water sample (USEPA,1999).

$$C = \frac{EMR}{V} \quad \text{.....4.1}$$

where; C is the radon concentration ($Bq/m^3$), E is the emanation coefficient; M is the total mass of the sample (kg); R is the radium activity concentration (Bq/kg) and V is the effective volume of the sampling device ($m^3$). The effective volume of the RAD 7 detector is determined by considering the volume of the closed vessel for all materials inside the closed vessel, of the loop system.

### 4.7.2 Mean Annual Effective Dose

To estimate the inhalation and ingestion doses, the levels of radon in water have posed a greater danger than other contaminants. Therefore, there is a need to calculate the Mean Annual Effective Dose (MAED) for ingestion using the given equation. (UNSCEAR, 2000)

$$D_{ig}(mSv.year^{-1}) = C_{Rn} \times C_w \times EDC \quad \text{.....4.2}$$

where $D_{ig}$ is the effective dose for ingestion, $C_{Rn}$ is the radon concentration in water (Bq $l^{-1}$ or kBq $m^{-3}$), $C_w$ is the weighted estimate of water consumption of 2 litres per day (60 l $y^{-1}$) and *EDC* is the effective dose coefficient for ingestion (3.5 nSv $Bq^{-1}$) respectively.

### 4.7.3 Water to Air Dose Distribution

The effective dose in the air emanating from the water via inhalation was evaluated using equation 4.3 and parameters established in the (UNSCEAR, 2000) report.

$$D_{in}(mSv.year^{-1}) = A_{Rn} \times C_{aw} \times F \times I \times DCF \quad \text{.....4.3}$$

where $D_{in}$ is the effective dose via inhalation, $A_{Rn}$ is the radon concentration in water (Bq/L or kBq/$m^{-3}$), $C_{aw}$ is the radon in the air to the radon in water ratio ($10^{-4}$), $F$ is the equilibrium factor between radon and its progenies (0.4), $l$ is the average indoor occupancy time per individual (7000 $hy^{-1}$) and *DCF* is the dose conversion factor for radon exposure (9 nSv (Bq h $m^{-3}$)$^{-1}$ as in (UNSCEAR, 2000).

## 4.8 Sediment Sample Collection and Analysis

### 4.8.1 Materials

The following materials were used during the sample's collection, preparation, data acquisition and analysis; 15 plastic bottles every 500 ml for provisionally holding the bulk sediments from the wells, labelling stickers and marker pens for putting identity labels on the different samples to avoid cross-contamination. 15 standard plastic bottles of capacity 300 ml. Standard plastic bottles will be used for holding the geological sample matrix of the same volume as the standard samples. Oven drier for driving off any moisture content that might be present in the samples to enable the direct calculation of

the radioactive count due to the sediment only, grinding machine for pulverizing the sediments to attain the homogeneity of radionuclides in the sample matrix and maximize the full filling capacity of the sample, digital weighing machine for accurate measurement of the sediments, lining vinyl for sealing the caps to ensure radon gas and its daughters doesn't leak, high-resolution gamma-ray spectrometer coupled to the necessary electronics with pre-installed emulation software for spectral recording and analysis.

### 4.8.2 Collection of Sediment Samples

Sediments from 5 shallow wells and 10 boreholes were collected from the base of the well or soil excavated from the boreholes using a plastic container.

The sediments are believed to have weathered from the rocks bearing the water aquiver underground. The soil was collected up to a depth of 50 cm to a maximum of *1 m a*round the borehole to ensure proper mixing to get equilibrium. The samples were packed into a clean non-radiating bottle of 500 ml and transported for preparation.

### 4.8.3 Sample preparation

15 well-labeled sediment samples from different water wells and boreholes in Mutomo Sub County were packaged in clean bottles with airtight clean bottles to avoid cross-contamination and taken to the laboratory for preparation at the Ministry of Mining and Petroleum the Republic of Kenya.

The samples were air-dried individually before oven drying them for 24 hours at a temperature of 105 °C in a closed oven after which they were then ground to a fine powder to ensure homogeneity of the radioactive species present. The samples were then taken to the institute of nuclear science and technology, of the University of Nairobi where a mass was 275g of the bulk sample was accurately transferred to a standard plastic beaker. The caps of the standard plastic beaker were lined with aluminium foil to ensure that radioactive gases do not leak.

The samples were given an identification tag bearing, the name, mass of the sample and date of preparation. The samples were kept for a minimum of 28 days to attain secular equilibrium before counting.

### 4.9 HPGe Detector: Operational Characterization

The detector is made from Germanium, a group IV element due to its small energy gap. HPGe detector transforms gamma energy directly into electron-hole pairs. The resulting charge carriers within the depletion region are swept by the electric field due to the presence of reverse bias voltage across the collection electrodes. The charges are converted into electric pulse which has a linear dependence on gamma energy deposited (Krane, 1988). The HPGe detector used in this work is closed-ended with a coaxial geometry, which maximized charge collection. The detector frontal surface is a thin planar surface, which minimizes attenuation of the weak gamma rays from the geogenic sample under the study (Knoll 2010). Due to the small energy gap, slight thermal agitation of the electrons excites electrons from the valence band to the conduction band and this is recorded as an electric pulse, an effect that lowers the superior resolution of the HPGE detector. To minimize leakage current due to thermal excitation of the electrons, the detector crystal is cooled to lower the energy of the electrons. This is achieved by keeping the crystal in liquid nitrogen at - 196°C in a well-insulated dewer.

#### 4.9.1 Energy Calibration

Energy calibration is a fit from the plot of channel numbers (y-axis) and photon energy in keV (x-axis). The calibration fit is plotted is from the points from standard sources certified by IAEA.

The fit relates known peak energies to specific channel numbers, which converts the channel numbers from spectra recorded from geological sources to energies for identification purposes (Gilmore, 2008). To identify and quantify the radionuclides present in a geological sample, a standard sample whose energies are $^{241}$Am, $^{60}$Co and $^{40}$K with peak energies 59.5 keV, 1332 keV and 1460 keV. A second-order polynomial fit

is done over the plot of channel numbers versus the peak energies from the standard sources. The linear fit was used to convert channel numbers to energies for gamma lines from $^{214}$Pb, $^{214}$Bi, $^{212}$Pb, $^{228}$Ac and $^{40}$K at 351 keV, 609 keV, 238 keV, 911 keV and 1460 keV respectively. The standard sample was chosen because its energy range covers the energy range of peaks of interest from geologic samples which is a requirement for the satisfactory precision of the data (IAEA, 2007).

### 4.9.2 Detector Efficiency (ε)

It is a routine quantity control prerequisite in gamma spectroscopy. Counting efficiency gives the probability that an emitted gamma-ray will interact with the detector crystal and produce a count (Reguigui *et al.,* 2006). The detection of neutral particles like gamma and alpha is not prompt as they must travel some distance and interact to transfer their energy so that they can be detected. Sometimes they may fail to interact which decreases the ratio of detected photons to the incident photons (Full energy peak efficiency). The detector efficiency is dependent on detector crystal size, the detector-source geometry and the nature of the casing material. The photo-peak efficiency for detecting $^{238}$U, $^{232}$Th and $^{40}$K were calculated from Certified Reference Materials (CRM) RG-series as RGK-1, RGU-1, and RGTh-1 traceable by the International Atomic Energy Agency (IAEA).
Equation 4.1 below was used in the calculation of the photopeak efficiency.

$$A_c = \frac{N_D}{\rho.\eta.m} \quad \text{.....(4.4)}$$

Where; $\eta$ is the detection efficiency (photopeak) at particular gamma-ray energy $E_\gamma$. $N_p$ - is the net gamma-ray count at the full energy peak, $A$- represents the activity of the standard source in Bq and for this study was 4,940 Bq/Kg, 3,250 Bq/Kg and 14,000 Bq/Kg for $^{238}$U, $^{232}$Th and $^{40}$K respectively. $P_\gamma$ -is the standard gamma decay probabilities given by International Atomic Energy Agency (IAEA, 2007), as 0.3534, 0.4516, 0.4316, 0.258 and 0.1066 for $^{214}$Pb at 351 keV, $^{214}$Bi at 609 keV, $^{212}$Pb at 238 keV, $^{228}$Ac at 911 keV and $^{40}$K at 1460 keV respectively. $t$ -is the counting live time (s).

### 4.9.3 Detector Resolution

Detector resolution measures the ability of the detector to record distinctively two peaks of close energies. High detector resolution increases the quality of the data. It determines the full width at half maximum (FWHM) of energy peak at specified energy. The energy resolution of the HPGe detector is affected by background emissions and electronic noises. To maintain high resolution for HPGe, the germanium crystal is cooled to below 77 K to minimize the thermal agitation of electrons.

The detector crystal is made of high purity germanium because of its small forbidden gap which makes it suitable for the detection of low gamma energies (Reguigui *et al.*, 2006). The detector resolution was determined using equation 4.2.

$$R = \frac{FWHM}{H_0} \times 100\% \quad \text{.....4.5}$$

Where; FWHM is the full width of the energy peak at its Half Maximum and Ho is the channel number corresponding to the centroid of the peak.

### 4.9.4 Background Correction

The background count was evaluated by counting de-ionized water in the same geometry as the geogenic sample. The background count from the spectrum was essential for correcting the spectrum from each sample. Background correction is necessary for quality control. To maintain the quality of the data on radioactivity, it is, therefore, necessary to subtract the background count from the measured gross count to obtain the net activity of each sampled sample.

### 4.10 Sediments Dosimetric Quantities

The sediment samples were analyzed for the following quantities; Activity concentration of $^{226}$Ra, $^{232}$Th and $^{40}$K, Radiation hazard indices (radium equivalent, external and internal hazard indices), absorbed dose rate and annual effective dose rate.

### 4.10.1 Activity Concentration ($A_c$)

The radionuclides from the 238U and 232Th series were detected from the gamma lines of their short-lived decay products, namely (214Bi & 214Pb) and (212Pb & 228Ac), after running separately all the prepared rock and sand samples in the spectrometer. From its solitary photo-peak at 1460 keV, 40K was detected. After background correction, the relative abundance of the radioactive species of interest in all samples was determined from the spectrum to be 46. Equation 4.6 proposed by Ebaid (2010) was used to compute the specific activity concentration of 238U, 232Th, and 40K in the sand and rock samples using measurements of net counts (Bq), sample mass (Kg), counting live time(s), and detector efficiency response.

This is the activity of a substance that contains a radionuclide per unit mass (Gilmore, 2008). The analytical formula used to determine the radionuclide activity concentrations in Bqkg-1 is shown in equation (4.6). (Ebaid, 2010).

$$A_c = \frac{N_D}{\rho.\eta.M} \quad \text{.....(4.6)}$$

Where $N_D$ is the net counts of the radionuclide in the samples, $p$ is the gamma-ray emission probability (gamma-ray yield), $\eta\ (E)$ is the absolute counting efficiency of the detector system, $T_c$ is the sample counting time, m is the mass of the sample (kg).

### 4.10.2 Absorbed dose (D)

The absorbed dose was evaluated using activity to dose conversion factors ($nGy^{-1}$ per Bq/Kg) of 0.427, 0.662 and 0.043 for $^{226}Ra$, $^{232}Th$ and $^{40}K$ respectively as provided by UNSCEAR 2000. Equation 4.6 was used in the determination of the dose rate.

$$D\ (nGyh^{-1)} = 0.427C_{Ra} + 0.662C_{Th} + 0.043C_K \quad \text{.....(4.7)}$$

Where: $C_{Ra}$, $C_{Th,}$ and $C_K$ are the average activity concentration of $^{238}U$, $^{232}Th$, and $^{40}K$ in $Bqkg^{-1}$, respectively in the homogeneous sample of rock and sand samples.

### 4.10.3 Radium Equivalent ($Ra_{eq}$)

Radium equivalent refers to the weighted sum of the activities of $^{232}Th$, $^{226}Ra$ and $^{4}He$ based on the assumption that 1 Bq/Kg of $^{232}Ra$, 0.7 Bq/Kg of $^{222}Ra$ and 13 Bq/Kg of $^{4}He$ deliver the same gamma dose rate (Beretka and Matthew, 1985).

Equation 4.8 was used for calculating the radium equivalent;

$$Ra_{eq} = C_{Ra} + 1.423C_{Th} + 0.077C_{K} \quad (4.8)$$

Where $C_{Ra}$, $C_{Th}$ and 0.077 $C_k$ are the activity concentrations of $^{226}Ra$, $^{232}Th$ and $^{40}K$ respectively. For safety, any construction material with $Ra_{eq}$ >370 Bq/kg should not be used as it poses a radiation exposure hazard. (UNSCEAR, 2008).

### 4.10.4 Radon Equivalent ($Rn_{eq}$)

Radon equivalent refers to the weighted sum of the activities of $^{222}Rn$, $^{218}Po$ and $^{4}He$ based on the assumption that 1 Bq/Kg of $^{222}Rn$, 0.3 Bq/Kg of $^{218}Po$ and 37 GBq/Kg of $^{4}He$ deliver the same gamma dose rate (Beretka and Matthew, 1985). Equation 4.8 shows the empirical formula to be used for calculating the radon equivalent;

$$Rn_{eq} = (0.106\, c_{Po\text{-}218} + 0.514\, c_{Pb\text{-}214} + 0.380\, c_{Bi\text{-}214}) / c_{Rn\text{-}222} \quad (4.9)$$

Where; c stands for the activity concentration of radon and its average globally outdoor radon levels range between 5-15 Bq/$m^3$, which equals 0.135-0.405 pCi/L. meaning that every 99.9 Bq/$m^3$ or every 2.7 pCI/L may lead to cancer if it increases in long-term exposure to radon.

# CHAPTER FIVE

## 5.0 RESULTS AND DISCUSSION

### 5.1 Introduction

This topic presents the researcher's findings on the level of radon in underground water in the Mutomo area, Kitui County. The study further presents radiometric analyses of radium levels in sediments sampled from the bottom of the shallow wells or the proximity in the case of the borehole and springs. The correlation between radium in sediments and radon in water has been evaluated and presented. The present results are compared with the published findings and reference levels suggested by radiation regulatory bodies.

### 5.2 Analysis of Water Samples

#### 5.2.1 Radon Concentration in Water

The data on radon levels from three categories of underground water sources namely, boreholes (some boreholes were operated using machines denoted by **BMO** whiles others were hand-operated denoted by **BHO**), wells and springs were evaluated using a RAD 7 alpha detector. The detector is made of semiconductor material, which converts alpha radiation to electrical energy. In this work, radon from various water sources will be presented. The various water sources, their geo-reference coding and the level of radon concentration in $kBq/m^3$ have been summarized in Table 5.1

**Table 5.1: Radon concentration in kBq/m$^3$ from various water samples**

| S/no | Sample Name | Geo- Reference | Water source | Radon in kBqm$^{-3}$ |
|---|---|---|---|---|
| **1** | **Munyoki A** | 38.37 S 1.81E | Well | ND |
| **2** | **Kasiluni** | 38.38 S 1.80E | BMO | 47±2.4 |
| **3** | **Kavuse** | 38.39 S 1.80E | BHO | 28±14 |
| **4** | **Ngosini** | 38.41 S 1.79E | Spring | 120±6 |
| **5** | **Mutha town** | 38.42 S 1.80E | BHO | 54±2.7 |
| **6** | **Kawambemba** | 38.42 S 1.79E | BMO | 18±0.9 |
| **7** | **Yimikoongoo** | 38.35 S 1.82E | BMO | 32±1.6 |
| **8** | **Katuuni** | 38.30 S 1.88E | Well | ND |
| **9** | **Musila** | 38.31 S 1.81E | Well | ND |
| **10** | **Kyanga** | 38.36 S 1.79E | BMO | 17±0.85 |
| **11** | **Makutano** | 38.36 S 1.75E | BHO | 52±2.6 |
| **12** | **Muliluni** | 38.38 S 1.80E | BMO | 23±1.2 |
| **13** | **Kwa Nzalu** | 38.40 S 1.79E | Well | 14±0.7 |
| **14** | **Munyoki B** | 38.37 S 1.80E | Well | 11±0.55 |
| **15** | **Kwithima** | 38.31 S 1.77E | BHO | 27±1.4 |
| | **MEAN** | | | **30±1.5** |

The findings show that radon levels varied for each source despite the same empirical controls during radon measurements. This variation was inferred to a wider spacing of sampled water sources could have led to geological variation since it is a key contributor to radon levels. Furthermore, the water samples were not collected along any geological profile line rather they were collected randomly from different villages. The water sample was collected from underground water whereby the residents relied on it for domestic purposes. Since the aim was to determine Radon levels on those specific water sources point. Radon in water ranged from below detection level (BDL) = kBqm$^{-3}$ for shallow wells to 120±6 kBqm$^{-3}$ for water sampled from a spring at the bottom of the Mutha. The undetectable levels of radon in well waters (Munyoki, Katuuni and Katuuni) were attributed to disturbance of water leading to dissolution/desorption of radon from water

leading to evaporation or mineral leached to lower levels. To minimize radon evaporation, the water was sampled in the morning and the late evening and the radon measurements were done onsite immediately but it also resulted in resulted to a below detectable level(BDL). This indicated no presence of Radon concentration in those areas. The level of radon in water is temperature-dependent and radon dissolved in water decreases with an increase in temperature (Duggai *et al.*, 2013). However, Kwanzalu and Munyoki B wells reported average radon levels of 14±0.7 and 11±0.55 $kBqm^{-3}$ respectively. This was inferred by their depth and granitic rocky background which in the past has led to radium enrichments in water (Hystad *et al.*, 2014).

Radon levels in all the boreholes were detectable with a range of 17±0.85 to 54±2.7 $kBqm^{-3}$ with a mean of 33±1.7 $kBqm^{-3}$. Mean radon concentration from boreholes, surpassed the recommended value of 11 Bq/L by the US Environmental Protection Agency, USEPA. Higher radon levels from borehole water were attributed to radium enrichments in underground waters by granitic rock systems bordering the aquiver (Choubey *et al.*, 2001). Figure 5.1 presents radon levels from various water sources.

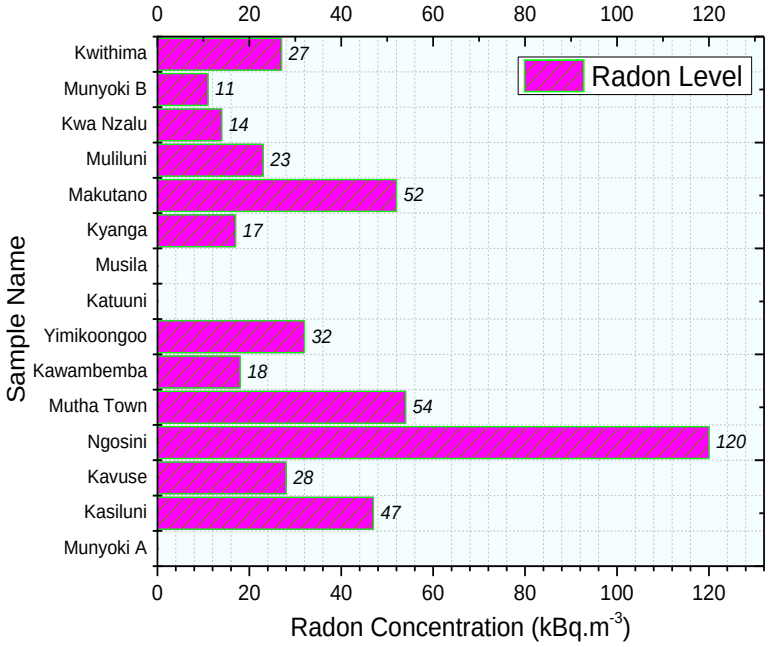


**Figure 5.1: Radon concentration in water in $kBqm^{-3}$ for a variety of both shallow wells and boreholes**

The maximum radon level was reported from a spring in Ngosini village (120±6 $kBqm^{-3}$) which lies, on the slopes of Mutha hill where there is a blend of igneous and metamorphic rocks and water was oozing as being collected. Radon gas could thus dissolve in water diffusing through the veins of the rocks and accumulate to high levels as shown in figure 5.1. The mean radon concentration in water from the area of study is averaged to 30±1.5 $kBqm^{-3}$ which lies within the recommended range of 4 - 40 $kBqm^{-3}$ recommended by UNSCEAR, 2000. However, some boreholes and springs (Kalisuni, Ngosini, Mutha town, and Makutano) have radon levels higher (Table 5.1) than the recommended values. This was attributed to the geological composition of the region which is ingenious and metamorphic rocks. Figure 5.1 further shows that underground waters have reported higher levels of radon compared to surface waters more so where the aquiver is within or in the neighbourhood of metamorphic or granitic rocks since radon concentrations vary widely with the geographical area (Hystad *et al.*, 2014).

In addition, water from boreholes is enclosed, thus there is minimal radon diffusion into the atmosphere leading to accumulation to higher levels. In conclusion, the measured value of radon concentration was in a reasonable range with a recommended maximum radon concentration value of 100 Bq/L suggested by (WHO 2004; EC 2001).

### 5.2.2 Annual Indoor Effective Dose from water

To assess the potential harmful biological effects due to radon in water consumed in this area, the annual effective dose was evaluated using equation 4.2. Annual effective dose varied correspondingly as radon activity for various water sources. Table 5.2 presents average annual effective doses from a variety of water sources sampled.

**Table 5.2: Indoor annual effective dose rate emanating from water Sampled from various water sources**

| S/no | Sample Name | Geo- Reference | Water source | Indoor AED (mSv $y^{-1}$) |
|---|---|---|---|---|
| **1** | **Munyoki A** | 38.37 S 1.81E | Well | 0±0 |
| **2** | **Kasiluni** | 38.38 S 1.80E | BMO | 0.009±0.0004 |
| **3** | **Kavuse** | 38.39 S 1.80E | BHO | 0.005±0.0002 |
| **4** | **Ngosini** | 38.41 S 1.79E | Spring | 0.025±0.0012 |
| **5** | **Mutha town** | 38.42 S 1.80E | BHO | 0.011±0.0005 |
| **6** | **Kawambemba** | 38.42 S 1.79E | BMO | 0.003±0.0001 |
| **7** | **Yimikoongoo** | 38.35 S 1.82E | BMO | 0.006±0.0003 |
| **8** | **Katuuni** | 38.30 S 1.88E | Well | 0±0 |
| **9** | **Musila** | 38.31 S 1.81E | Well | 0±0 |
| **10** | **Kyanga** | 38.36 S 1.79E | BMO | 0.003±0.0001 |
| **11** | **Makutano** | 38.36 S 1.75E | BHO | 0.01±0.0005 |
| **12** | **Muliluni** | 38.38 S 1.80E | BMO | 0.004±0.0002 |
| **13** | **Kwa Nzalu** | 38.40 S 1.79E | Well | 0.002±0.0001 |
| **14** | **Munyoki B** | 38.37 S 1.80E | Well | 0.002±0.0001 |
| **15** | **Kwithima** | 38.31 S 1.77E | BHO | 0.005±0.0002 |
| | **MEAN** | | | 0.006±0.0003 |

The effective dose taken via inhalation ranged from 0 $mSvy^{-1}$ to 0.025±0.0012 $mSvy^{-1}$ with an average of 0.006±0.0003 $mSvy^{-1}$. The mean effective dose reported in this study is, however, below the permissible limit reference level of 1.15 $mSvy^{-1}$ for drinking water suggested by the World Health Organization (WHO, 2000) and the European Council (EC, 2001). Based on WHO recommendations that if AED for drinking water is below 1.15 $mSvy^{-1}$ hence the population cannot be exposed to radiation that can course harm hence remediation measures may not be necessary thus, the water is termed safe for drinking purposes. In case AED is above the recommended limit of 1.15 $mSvy^{-1}$ then water should be treated before being used by the resident.

Ingestion of radon and its decay daughters exceeding 100 $\mu Svy^{-1}$ has reported some negative health consequences, particularly the risk of stomach cancer (Tabar *et al.*, 2014). The range and the average values of AED are useful in the protection of the public against excessive doses of radiation.

For this research, the levels of dissolved gases in water are below the safe limit and the welfare of the population that uses this water in the context of radiological protection is guaranteed. The variation of effective doses with the water source is represented in figure 5.2.

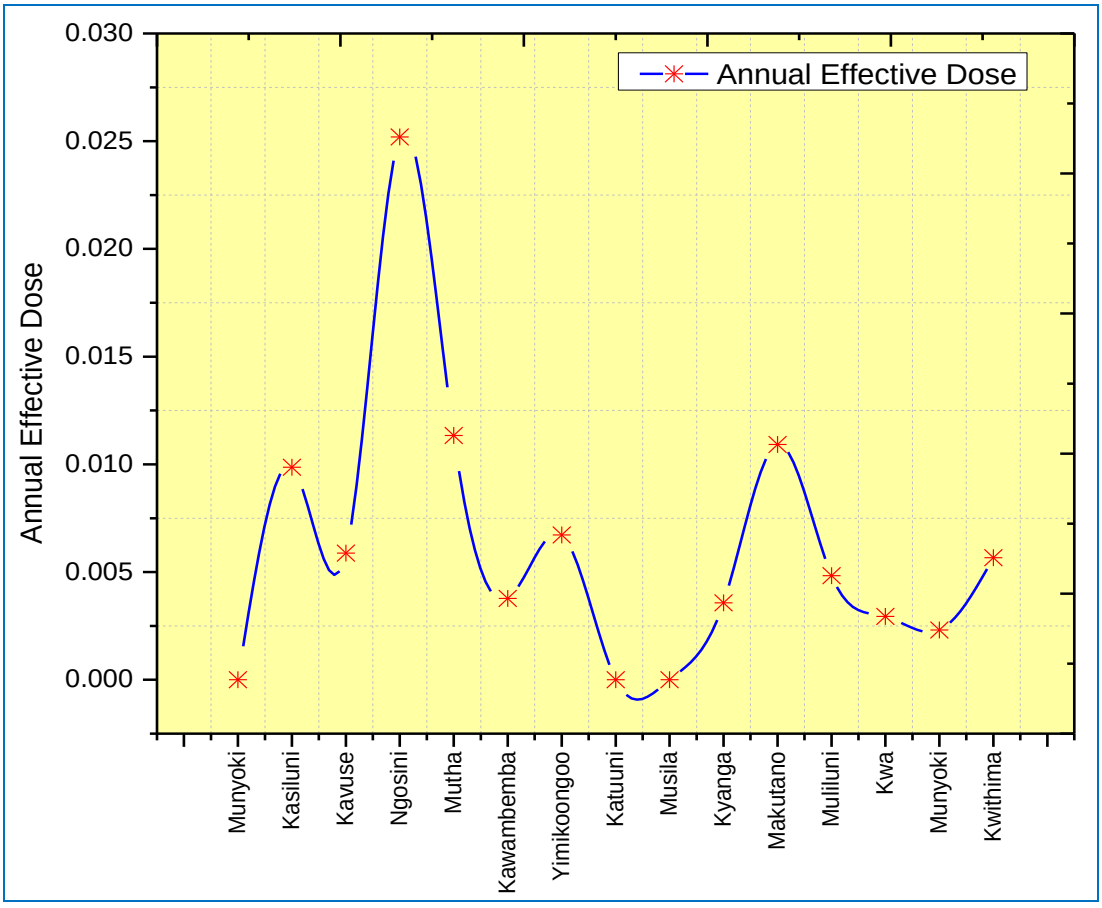


**Figure 5.2: Annual Effective Dose Rate from various water sources**

The individual sample's average and the overall mean reported by this work was well below the WHO reference level of 100 $Bqm^{-3}$ and based on this dosimetric quantity, the

use of this water purposely for drinking contributes an insignificant dose to cause harm to the population via ingestion.

### 5.2.3 Water to Air Dose Distribution

The evaluation of radon ($^{222}Rn$) released into the air was carried out using equation 4.3 and presented in figure 5.3

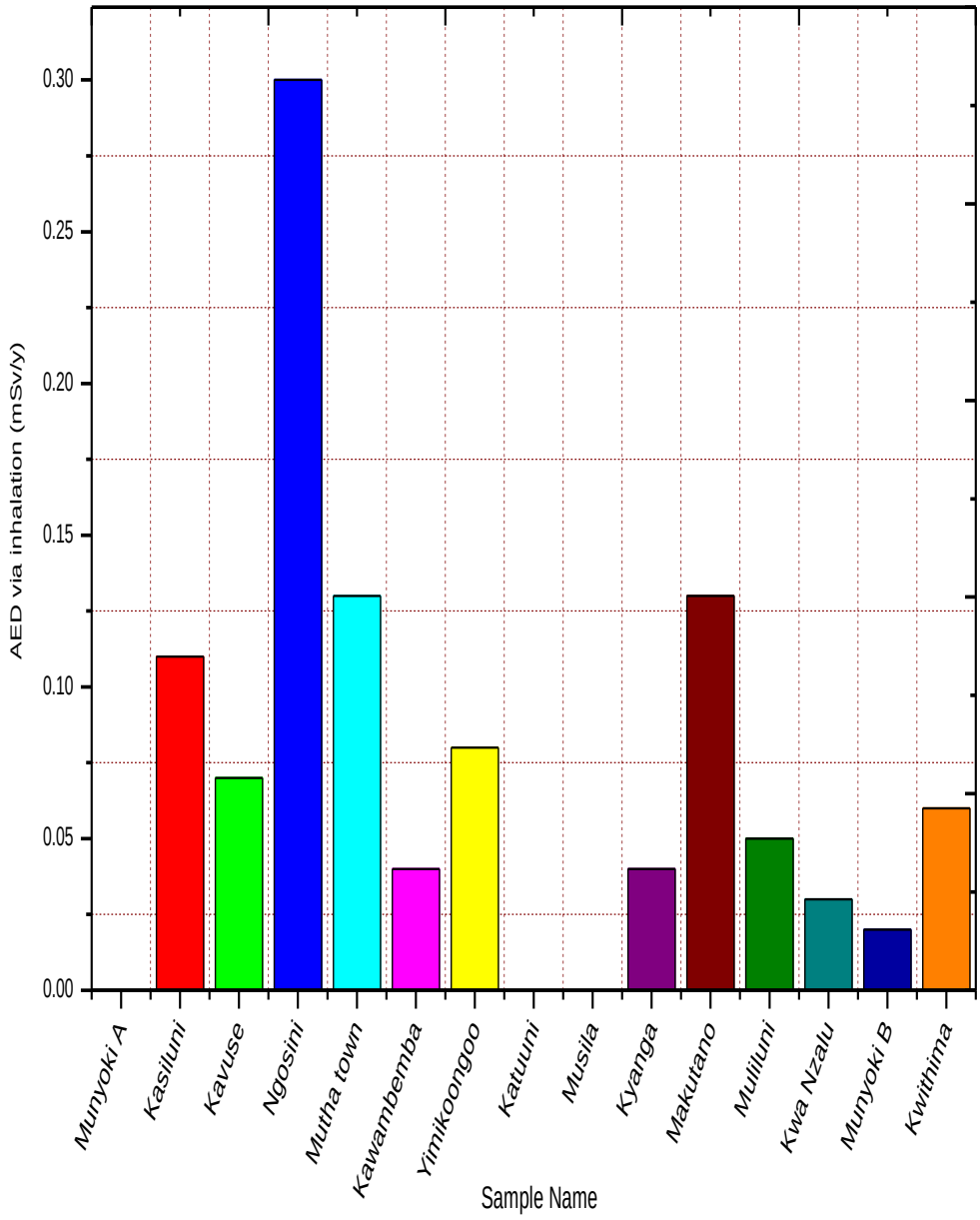


**Figure 5.3: Water to air dose distribution reported from various boreholes**

The dissolved radon gases from water contribute 70 % of indoor radiation. (Tabar *et al.*, 2014). This work, therefore, evaluated the indoor radiation dose released from the water and reports a minimum of 0±0 $mSvy^{-1}$ to a maximum of 0.3±0.015 $mSvy^{-1}$ with an average of 0.07±0.003 $mSvy^{-1}$ (Table 5.3).

**Table 5.3: Water to air dose distribution from various sources**

| S/no | Sample Name | Geo- Reference | Water source | Dose Distribution |
|---|---|---|---|---|
| **1** | **Munyoki A** | 38.37 S 1.81E | Well | 0±0 |
| **2** | **Kasiluni** | 38.38 S 1.80E | BMO | 0.11±0.005 |
| **3** | **Kavuse** | 38.39 S 1.80E | BHO | 0.07±0.003 |
| **4** | **Ngosini** | 38.41 S 1.79E | Spring | 0.3±0.015 |
| **5** | **Mutha town** | 38.42 S 1.80E | BHO | 0.13±0.006 |
| **6** | **Kawambemba** | 38.42 S 1.79E | BMO | 0.04±0.002 |
| **7** | **Yimikoongoo** | 38.35 S 1.82E | BMO | 0.08±0.004 |
| **8** | **Katuuni** | 38.30 S 1.88E | Well | 0±0 |
| **9** | **Musila** | 38.31 S 1.81E | Well | 0±0 |
| **10** | **Kyanga** | 38.36 S 1.79E | BMO | 0.04±0.002 |
| **11** | **Makutano** | 38.36 S 1.75E | BMO | 0.13±0.006 |
| **12** | **Muliluni** | 38.38 S 1.80E | BMO | 0.05±0.002 |
| **13** | **Kwa Nzalu** | 38.40 S 1.79E | Well | 0.03±0.001 |
| **14** | **Munyoki B** | 38.37 S 1.80E | Well | 0.02±0.001 |
| **15** | **Kwithima** | 38.31 S 1.77E | BHO | 0.06±0.003 |
| | **MEAN** | | | 0.07±0.003 |

The reported values were below the recommended level and that was a clear indication that the dose contribution in indoor air from water sampled in the studied water sources can be said to have levels of radionuclides hence safe**.**

## 5.3 Sediments Analyses

### 5.3.1 Detector Energy Calibration

Energy calibration helps to determine the level of energies from different peaks of the unknown spectrum that is used in qualitative analysis. A plot of photon peak energies of 59.5 keV, 1332 keV and 1460 keV from $^{241}$Am, $^{60}$Co and $^{40}$K respectively was done as shown in figure 5.4.

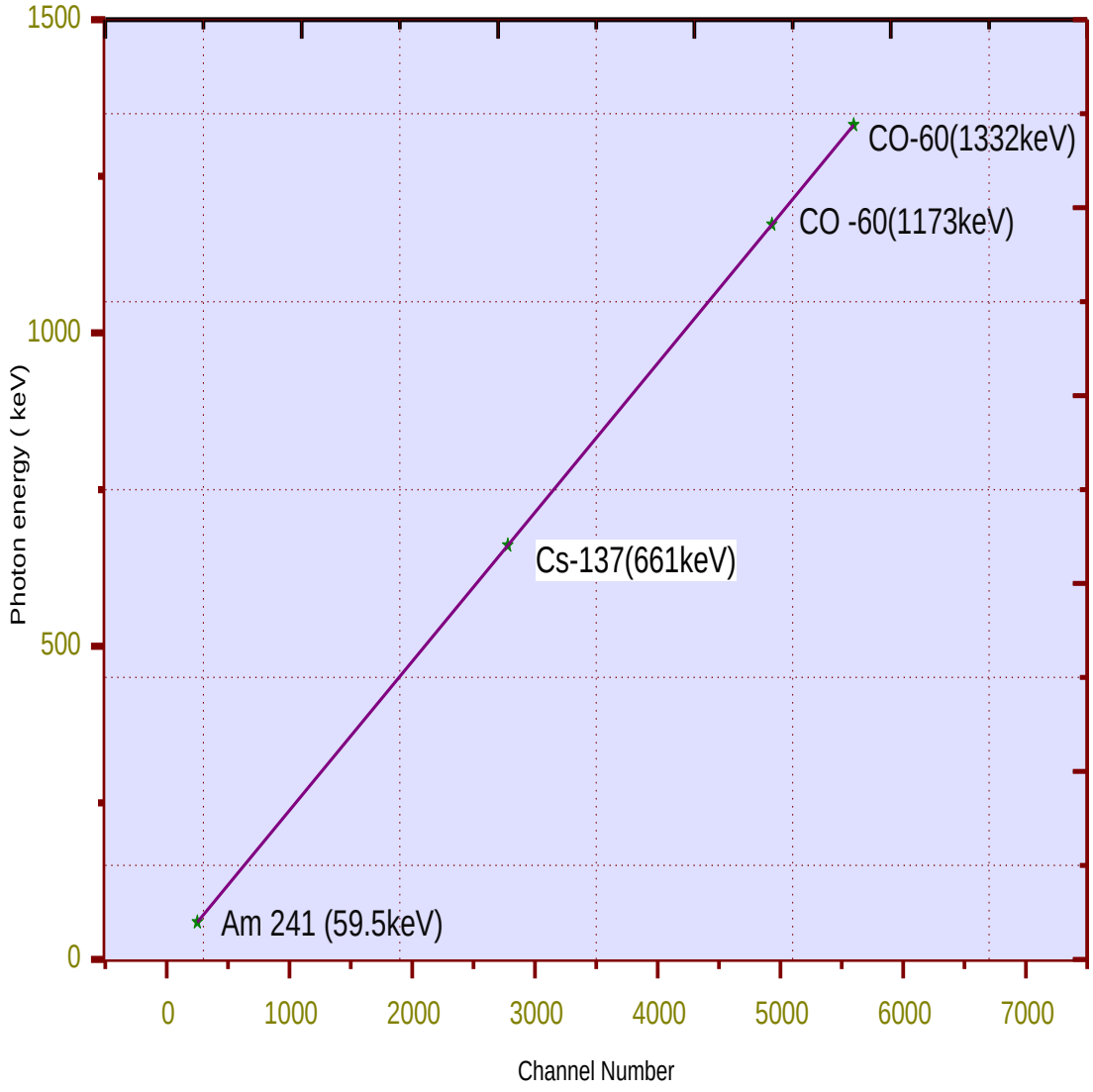


**Figure 5.4: Energy calibration fit used in this work done using sample source.**

The second-order polynomial fit of the general form $\boldsymbol{y(x)=A+Bx+Cx^2}$ was preferred due to precision more so at higher energies. From the polynomial, $y(x)=A+Bx+Cx^2$ , $y$ is the photon energy, $x$ is the channel number and A, B, and C are the fit parameters. The output of the equation $y(x)=A+Bx+Cx^2$ with the channel number known gives the channel energy (Shikali *et al*., 2014).

**Table 5.4: The polynomial and its fit parameters used during energy calibration**

Second order Polynomial $y(x)=A+Bx+Cx^2$

| **Parameter** | **Value** | **Standard Error** |
|---|---|---|
| A (Y-Intercept) | -0.12569 | ±0.31138 |
| B | 0.23763 | $\pm 2.74561 \times 10^{-4}$ |
| C | $5.5892 \times 10^{-8}$ | $\pm 4.58458 \times 10^{-8}$ |

From the second-order polynomial, y is the energy photon. While x is the number of the channel used to fit parameters: A, B and C.

### 5.3.2 Detector Efficiency

The detection efficiency of the HPGe detector was evaluated by plotting the detection efficiencies of gamma-ray photons of well-known energies versus varying energy of different full peak energies. The standard sources certified by IAEA were used during the recording of the full energy peak. Standard sources used for the efficiency calibration in this work include IAEA-RGK-1, IAEA-RGU-, and IAEA-RGTh-1 from IAEA.

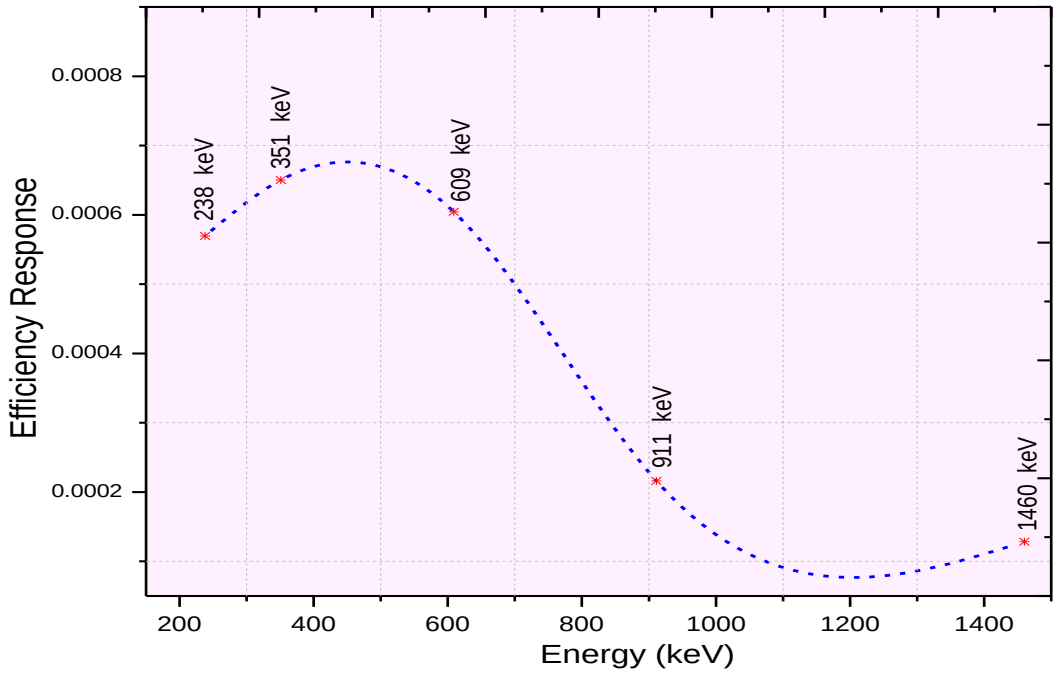


**Figure 5.5: Efficiency response curve for the HPGe detector used**

The detection efficiency at low energies is high due to full photon energy absorption through photoelectric absorption, which is the dominant mechanism at energies ranging between 0 and 100 keV, as can be seen from the plot of a detector's efficiency response at different gamma-ray energies (Debertin and Helmer, 1988). As the energy grows (from 100 keV to 1 MeV), Compton scattering takes over and scatters gamma-ray photons, some of which escape the detector without interfering, leading to low energy peaks and a drop in efficiency. A dramatic reduction in full energy 52 peak efficiency is observed above 1 MeV due to pair formation being dominant and a large proportion of incident gamma ray photons passing through the detector without interfering (5.5). A wide variety of energies can be covered by extrapolating the curve.

### 5.3.3 Detector Resolution

The detector resolution for this study was evaluated by fitting the $^{137}$Cs spectral peak at 661.5 keV as shown in Figure (5.6).

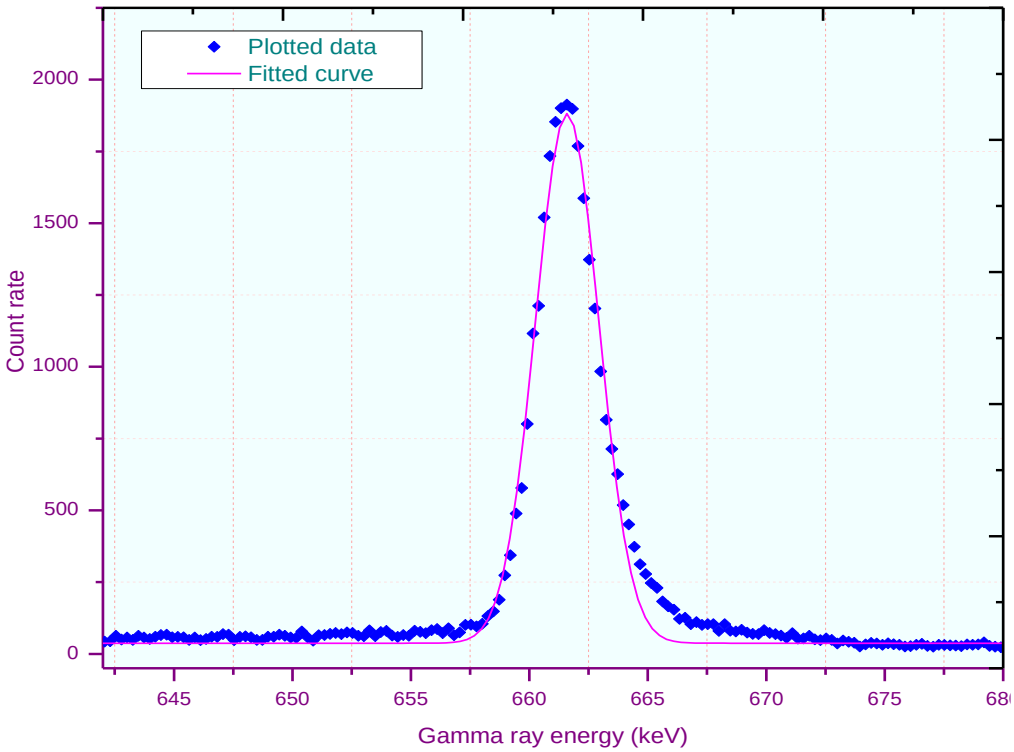


**Figure 5.6: Gaussian fit for $^{137}$Cs spectral peak at 661 keV**

The fit parameters from the Gaussian fit were generated and presented in Table (5.4)

$$y = y_0 + \frac{A}{w\sqrt{\frac{\pi}{2}}} \exp\left\{\frac{(-2(x-x_0)}{w^2}\right\}^2 \qquad 5.1$$

Where; $y_0$ represents the baseline offset of the peak (above the x-axis), $x_0$ is the peak centroid number, A is the net area under the peak, and w is the width of the peak at half maximum.

**Table 5.5: The Gaussian fit and fit parameters used to calculate detector resolution. The chi-square for the fitting was 0.97278**

| Parameter | Value | Standard error |
|---|---|---|
| $Y_0$ | 3.3587 | ±0.20940 |
| $x$ | 661.4943 | ±0.00886 |
| $A$ | 6301.6482 | ±35.8950 |
| $w$ | 38.2986 | ±0.77501 |

The percentage resolution (R) of the detector was calculated by substituting the values of $W$ and $X_0$ in the formula shown by equation (5.2)

$$R = \frac{W}{X_0} \times 100\% \quad \text{.....5.2}$$

Where; $W$ is the full width of the peak at half maximum given as 38±0.775 and $x_0$ - is the centroid peak (energy) whose fit parameter is 661±0.008 (Table 5.4). Based on the fit parameters, the detector resolution was established to be 5.6% at spectral photopeak of 661 keV of $^{137}$Cs. The current resolution of the detector was found to be in the reasonable range of practical detector resolution.

### 5.3.4 Background Corrections

The net count from the geogenic sample was obtained by correcting the gross count from the detector using the count recorded when only deionized water was in the detector volume. The equation 5.2 was used to obtain the net count used in this plot shown in figure 5.7

$$C_n = C_g - C_b \quad \text{.....(5.2)}$$

Where; $C_n$ is the net count rate of the sample, $C_g$ is the gross count from geological and non-geological sources. $C_b$, denotes the background count around the detector site. Figure 5.7 shows gross and net spectral data for sediment sampled from 38.36 S  1.75 E.

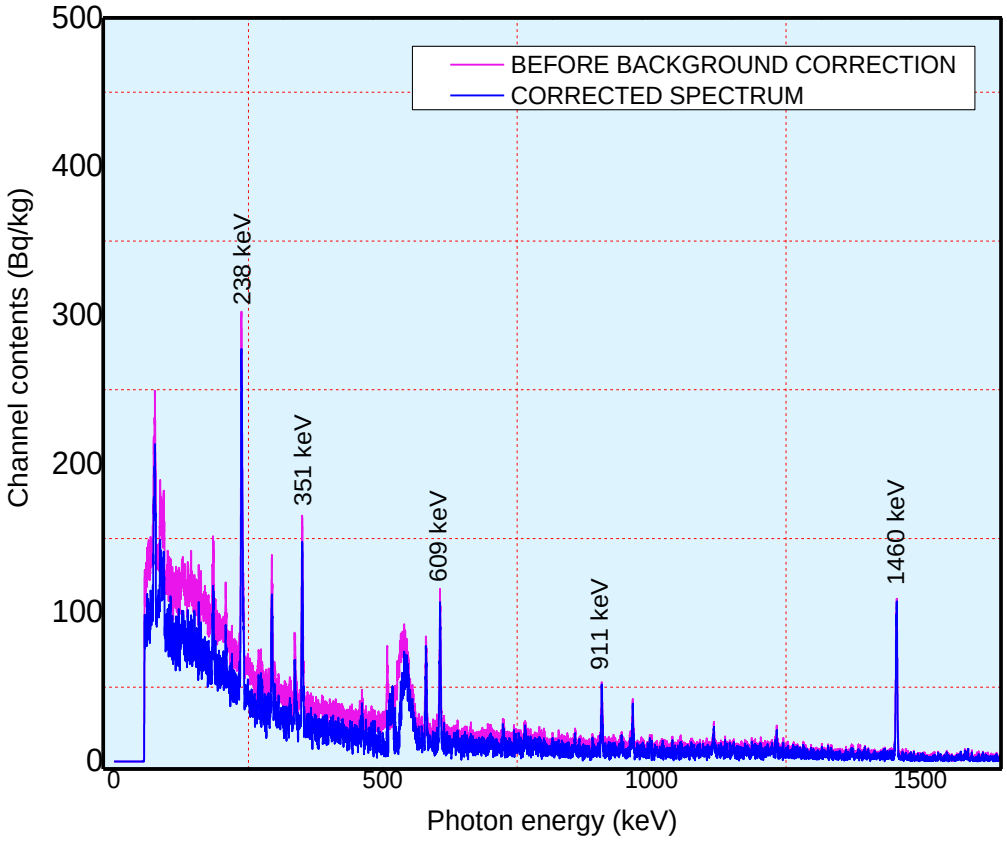


**Figure 5.7: Background corrected spectrum from a geogenic sample**

### 5.4 Analyses of Sediments Samples

The sediments samples collected from the different borehole and shallow wells were analyzed for the following quantities; Activity concentration of $^{226}Ra$, $^{232}Th$ and $^{40}K$, radium equivalent, absorbed dose rate and annual effective dose rate were calculated and presented in a tabular format below.

### 5.4.1 Activity Concentration (A)

**Table 5.6 Activity Concentration of $^{226}Ra$, $^{232}Th$ and $^{40}K$ in sediments samples from the basement of shallow wells and boreholes**

| Sample ID | Borehole/Well | $^{226}Ra$ | $^{232}Th$ | $^{40}K$ |
|---|---|---|---|---|
| **S01** | KATHATU | 13±0.67 | 18±0.94 | 1573±78.65 |
| **S02** | KATUUNI | 11±0.55 | 28±1.42 | 493±24.67 |
| **S03** | KAVUSYE | 26±1.32 | 45±2.25 | 819±40.99 |
| **S04** | KINAKONI | 15±0.79 | 22±1.12 | 631±31.55 |
| **S05** | KITONGA IKANGA | 27±1.36 | 62±3.1 | 786±39.31 |
| **S06** | KITUTA IKANGA | 19±0.96 | 83±4.19 | 949±47.46 |
| **S07** | KOOME IKANGA | 11±0.55 | 9±0.49 | 633±31.68 |
| **S08** | MULILUNI | 33±1.69 | 20±1.03 | 348±17.4 |
| **S09** | MUNYOKI A | 7±0.35 | 15±0.78 | 1034±51.71 |
| **S10** | MUNYOKI B | 54±2.74 | 9±0.47 | 1079±53.96 |
| **S11** | MUTHA-TOWN | 52±2.63 | 42±2.14 | 646±32.31 |
| **S12** | NGOSINI | 93±4.67 | 160±8 | 1741±87.07 |
| **S13** | NGOYOO | 225±11.26 | 24±1.24 | 964±48.21 |
| **S14** | NZALU-KANZIKO | 11±0.55 | 48±2.4 | 489±24.49 |
| **S15** | YIMIKONGOO | 19±0.95 | 42±2.12 | 713±35.68 |
| | **MEAN** | **41±2.07** | **42±2.11** | **860±43.01** |

The variation of the activity from one sample to the other was pegged to variation of the geological composition due to the vastness of the studied area and more so geological composition present in the parent rock. The fact that the samples were not collected from the same depth levels could also be a reason for the differences in the concentration of the considered radionuclides. The minimum $^{226}$ Ra concentration was reported from the sample obtained from Munyoki's shallow borehole as 7±0.35 Bq/Kg. A maximum activity concentration of 225±11.26 Bq/Kg was reported from a borehole known as Ngoyoo near Mutha market. The mean radium activity reported by the entire study was 41±2.07 Bq/Kg. $^{232}$Th ranged from 9±0.47 Bq/Kg to 83±4.19 with a mean of 42±2.11 Bq/Kg. $^{40}$K reported a mean of 860±43.01 Bq/Kg with a range of 348±17.4 Bq/Kg to 1741±87.07 Bq/Kg. The reported averages were above the world's averages of 33 Bq/Kg,

45 Bq/Kg and 400 Bq/Kg for radium, thorium and potassium respectively (UNSCEAR, 2008). The reported radium averages are inconsistent with the geology of Kitui County, which lies within the Central Eastern Mozambique Belt Segment (Nyamai *et al.*, 2003). The case of high $^{226}$Ra, $^{232}$Th, and $^{40}$K in Ngosini and Ngoyoo areas in Mutha could be due to the presence of Shale and Phosphate rocks, which dominates some parts of Kitui County (Mathu *et al.*, 2003). Figure 5.8 presents the activity concentration for the radium samples.

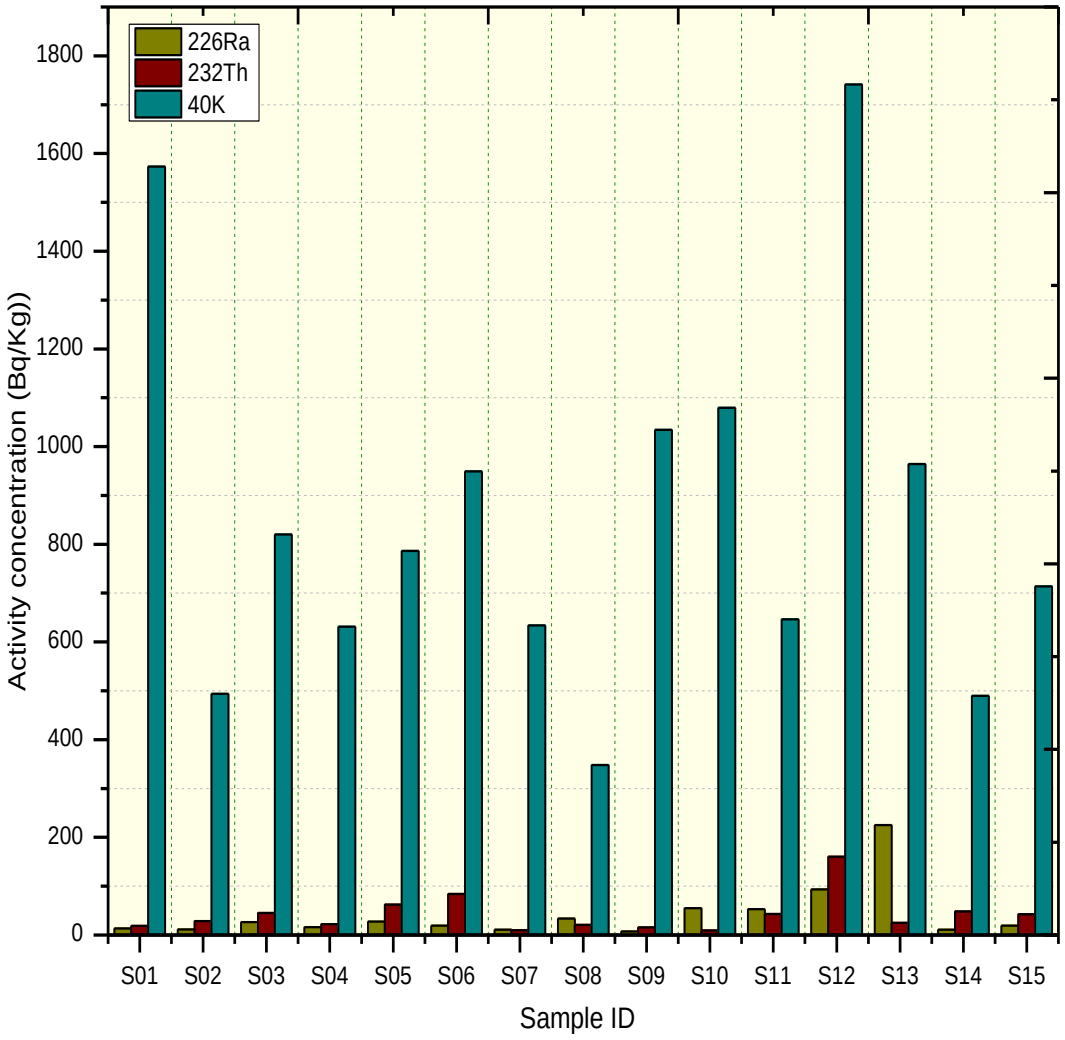


**Figure 5.8: Activity concentration of $^{226}$Ra, $^{232}$Th, and $^{40}$K in sediments sampled.**

### 5.4.2 Absorbed Dose (D)

The quantity of energy absorbed by human tissue was estimated by converting activity concentration to absorbed dose using equation 4.6 (UNSCEAR, 2000). The absorbed dose measured from the sample area varied spatially due to the non-uniform distribution of radionuclides in the earth's crust. The mean and range of doses are tabulated and presented in Table 5.6.

**Table 5.7: Absorbed doses from sediments samples collected from shallow boreholes**

| Sample's Name | Dose (nGy/h) |
|---|---|
| **Mutha-town** | 78±3.93 |
| **Nzalu-kanziko** | 57±2.87 |
| **Koome ikanga** | 38±1.92 |
| **Kinakoni** | 48±2.43 |
| **Kavusye** | 76±3.81 |
| **Muliluni** | 43±2.15 |
| **Munyoki A** | 57±2.89 |
| **Kituta ikanga** | 104±5.23 |
| **Kitonga ikanga** | 86±4.32 |
| **Katuuni** | 44±2.24 |
| **Ngoyoo** | 154±7.7 |
| **Ngosini** | 220±11 |
| **Kathatu** | 85±4.29 |
| **Yimikongoo** | 66±3.34 |
| **Munyoki B** | 76±3.8 |
| **MEAN** | 82±4.13 |

The studied area reported a mean absorbed dose of 82±4.13 nGy/h, which is above the world's mark of 60 nGy/h (ICRP, 2005; UNSCEAR, 2000). Sample collected at Ngosini (S12) figures 5.5 had the highest absorbed dose of 220±11.03 nGy/h thus contributing major radiation dose because of geological make-up of the region was mountainous and

rocky (Hystad *et al*,.2014) (see figure 5.9) on bar graph showing absorbed rate from different sample sediment collected. The majority of the sampled sediments had an absorbed dose that was slightly above the world's threshold value of 60 nGy/h thus contributing to the high doses.

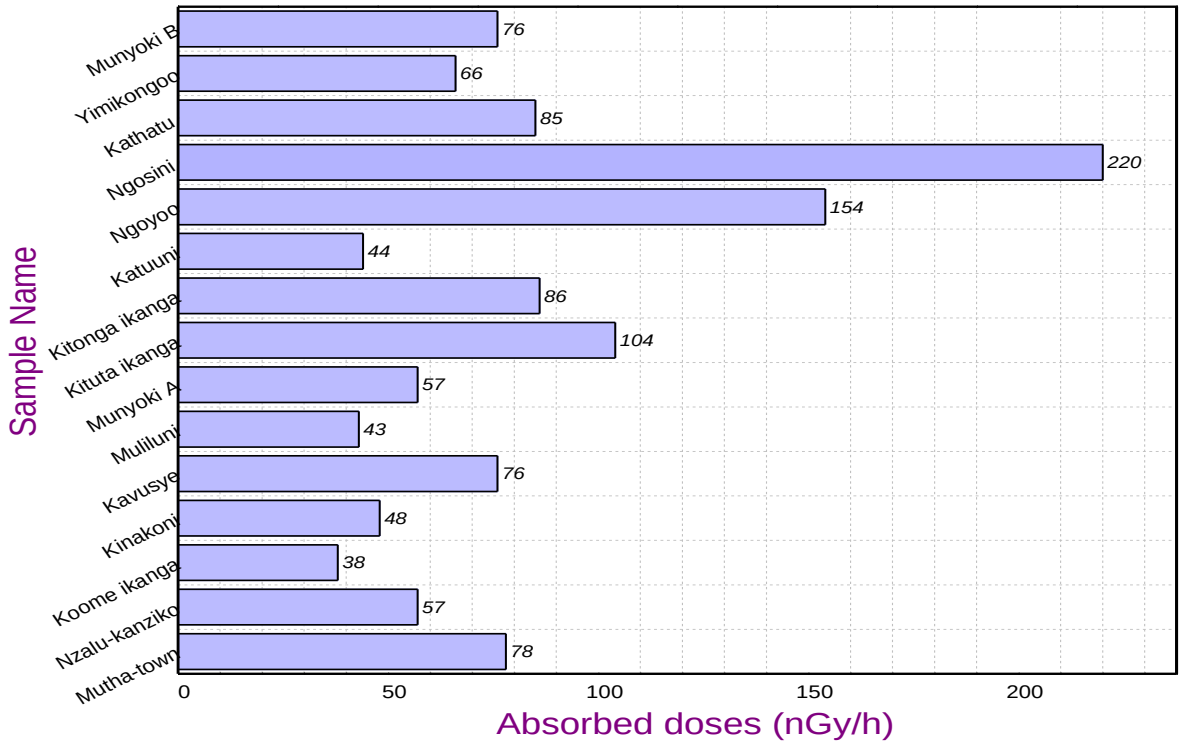


**Figure 5.9: Absorbed doses from sediments**

### 5.4.3 Annual Effective Dose Rate

The measure of the annual effective dose was evaluated by converting the absorbed dose. The AEDR measures the absorbed dose received by an individual over one year which evaluates the health risks to an individual (UNSCEAR, 2008). The higher the dose received by an individual, the higher the chances of harm it may cause to a healthy population. The levels of AEDR vary with activity concentration. Table 5.7 presents AED rates for the sampled areas.

**Table 5.8: Annual effective dose rate estimated from sediments collected from the sampled basement of shallow boreholes in Kitui South Sub County**

| Sample Name | AEDR (mSv/y) |
|---|---|
| **Mutha-town** | 0.19±0.009 |
| **Nzalu-kanziko** | 0.14±0.007 |
| **Koome ikanga** | 0.09±0.004 |
| **Kinakoni** | 0.11±0.005 |
| **Kavusye** | 0.18±0.009 |
| **Muliluni** | 0.1±0.005 |
| **Munyoki A** | 0.14±0.007 |
| **Kituta ikanga** | 0.25±0.012 |
| **Kitonga ikanga** | 0.21±0.01 |
| **Katuuni** | 0.11±0.005 |
| **Ngoyoo** | 0.37±0.018 |
| **Ngosini** | 0.54±0.027 |
| **Kathatu** | 0.21±0.01 |
| **Yimikongoo** | 0.16±0.008 |
| **Munyoki B** | 0.18±0.009 |
| **MEAN** | **0.2±0.01** |

Table 5.7 shows that the annual effective dose ranged from 0.09±0.004 mSv/y to 0.54±0.027 mSv/y with an average of 0.2±0.01 mSv/y. For a material to be termed to have negligible harm to the immediate population through exposure to radiations from natural sources, it should have a maximum annual dose limit of 1.15 mSv/y (UNSCEAR,2000)

Based on the findings from the present work, the mean radium effective dose reported from sediments from shallow wells, suggests it could be a low background area. Therefore, the materials are safe for human interaction.

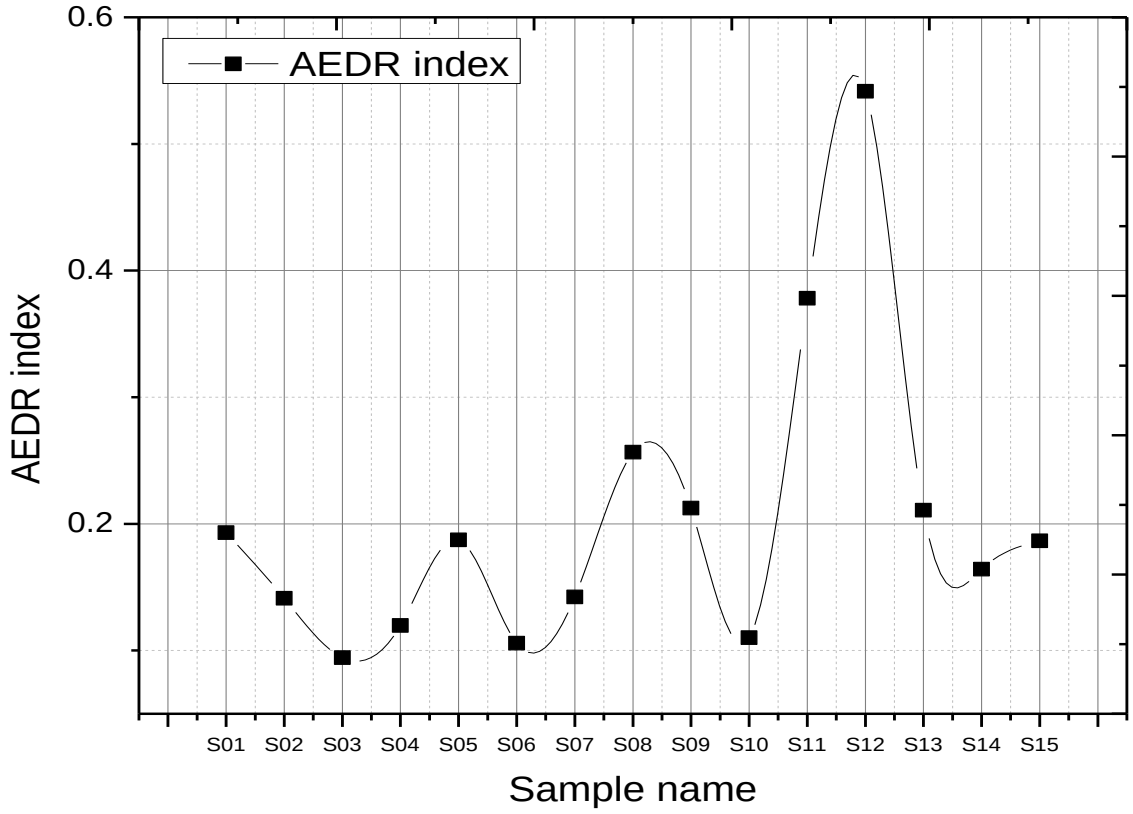


**Figure 5.10: Annual effective dose rate reported from sediments sampled from various boreholes within Mutomo Sub County, Kitui County**

The annual effective dose rate is instrumental in the estimation of the individual's potential radiation risks associated with interaction with radioactive material. Large quantities of the sampled sediments were from the basement sub strum and since it forms part of the aquifers, then elevated levels of radionuclides in rocks may have a high correlation with radon in water. This is possible because of the solubility of radium, thorium and potassium elements in the water. As the water, leaches to lower levels, its radionuclide and heavy mineral concentrations may change depending on the contents of the rocks along the soil profile. However, this study did both radon levels and radium concentration in water and soil sediments respectively. Figure 5.10 shows AEDR reported from sediments sampled from various boreholes within the Mutomo area.

### 5.4.4 Radium equivalent ($Ra_{eq}$)

There is non-uniform distribution of geogenic radionuclides, which were obtained by calculating of radium equivalent using equation 4.9. The measure of possible external radiation from primordial radionuclides particularly radium 226 was evaluated and presented in table 5.8.

**Table 5.9: Radium equivalent ($Ra_{eq}$)**

| Sample's Name | $Ra_{eq}$ (Bq/Kg) |
|---|---|
| **Mutha-town** | 163±8 |
| **Nzalu-kanziko** | 117±5 |
| **Koome ikanga** | 73±3 |
| **Kinakoni** | 96±4 |
| **Kavusye** | 153±7 |
| **Muliluni** | 90±4 |
| **Munyoki A** | 109±5 |
| **Kituta ikanga** | 211±10 |
| **Kitonga ikanga** | 176±8 |
| **Katuuni** | 89±4 |
| **Ngoyoo** | 335±16 |
| **Ngosini** | 455±22 |
| **Kathatu** | 161±8 |
| **Yimikongoo** | 134±6 |
| **Munyoki B** | 151±7 |
| **MEAN** | **167±8** |

Radium equivalent averaged 167±8.39 Bq/Kg with a lower limit of 73±3.69 Bq/Kg. only one sample was collected from Ngosini point (1.789150 S and 38.418240 E) which has a value of 455±22.76 Bq/Kg. This value surpassed the recommended limit of 370 Bq/Kq (ICRP, 2005). Figure 5.11 is a presentation of radium equivalent indices. The Ngosini borehole is located on a windward side of Mutha hill and is located down the hill

whereby there could have a variety of rock types present. The highest potassium content reported by this sample leads to its extreme deviation from the ranges of other samples. Silicate ores present in this area could be a reason for high Potassium minerals (Mustapha *et al.*, 2002).

All boreholes, except for Ngosini and Ngoyoo had low background radiation.

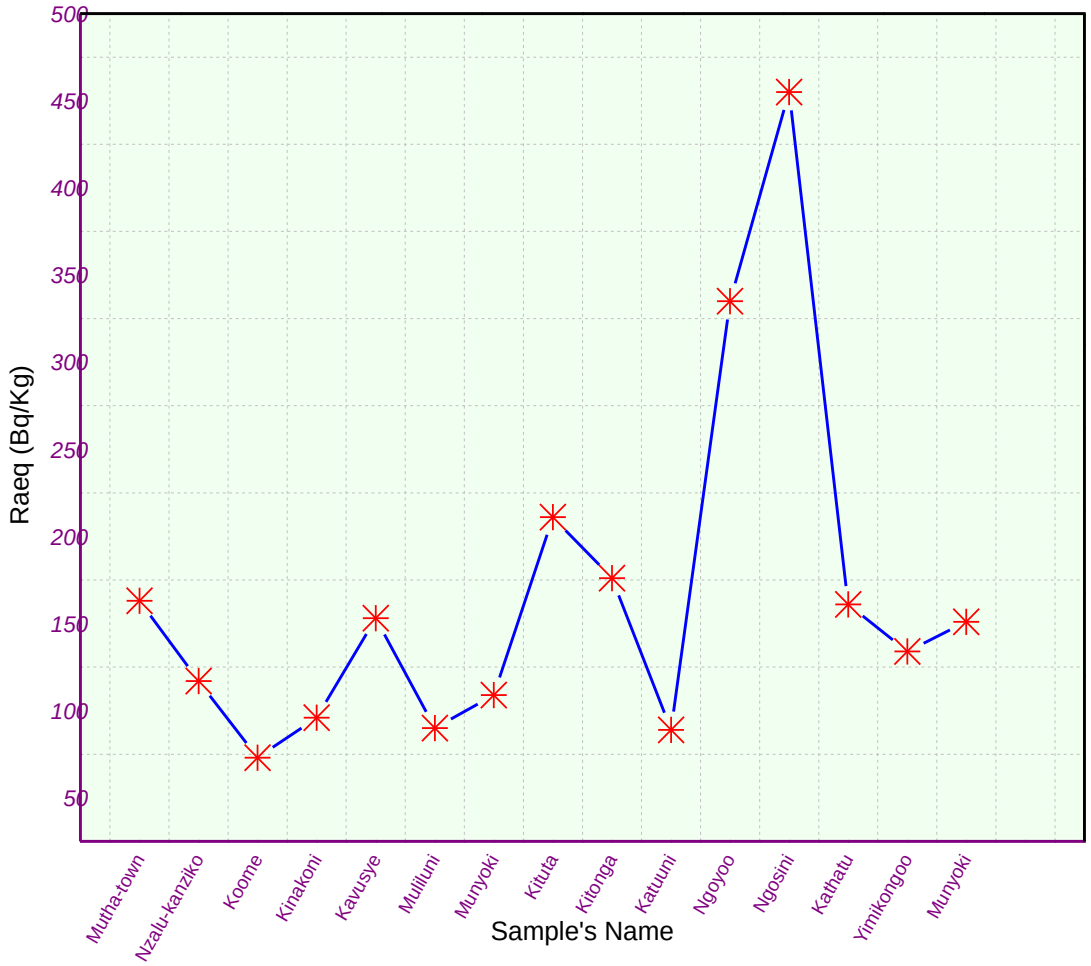


**Figure 5.11: Radium equivalent for sediments sampled from shallow wells and boreholes.**

**Table 5.10 showing correlation of results of underground waters and sediments**

| S/no | Sample Name | Radon in kBqm$^{-3}$ | $^{226}$Ra |
|---|---|---|---|
| **1** | Munyoki A | ND | 13±0.67 |
| **2** | Kasiluni | 47±2.4 | 11±0.55 |
| **3** | Kavuse | 28±14 | 26±1.32 |
| **4** | Ngosini | 120±6 | 15±0.79 |
| **5** | Mutha town | 54±2.7 | 27±1.36 |
| **6** | Kawambemba | 18±0.9 | 19±0.96 |
| **7** | Yimikoongoo | 32±1.6 | 11±0.55 |
| **8** | Katuuni | ND | 33±1.69 |
| **9** | Musila | ND | 7±0.35 |
| **10** | Kyanga | 17±0.85 | 54±2.74 |
| **11** | Makutano | 52±2.6 | 52±2.63 |
| **12** | Muliluni | 23±1.2 | 93±4.67 |
| **13** | Kwa Nzalu | 14±0.7 | 225±11.6 |
| **14** | Munyoki B | 11±0.55 | 11±0.55 |
| **15** | Kwithima | 27±1.4 | 19±0.95 |

Radon and radium belong to the same decay series $^{238}$U. $^{226}$Ra is a predecessor of $^{222}$Rn. Naturally, zones with predominantly high radium report high radon content (Mutungi, 2018: Hystad *et al,*.2014).

The current research tested the relationship between radon in water and corresponding radium in sediments. A scatter plot of radium from sediments was done against radon in water. A linear fit reveals a very weak positive relationship between radium (sediments) and radon from boreholes water. Figures 5.12 shows the scatter plots with a linear fit.

### 5.5 Correlation between $^{226}$Ra in Sediments vs. $^{222}$Rn in Water

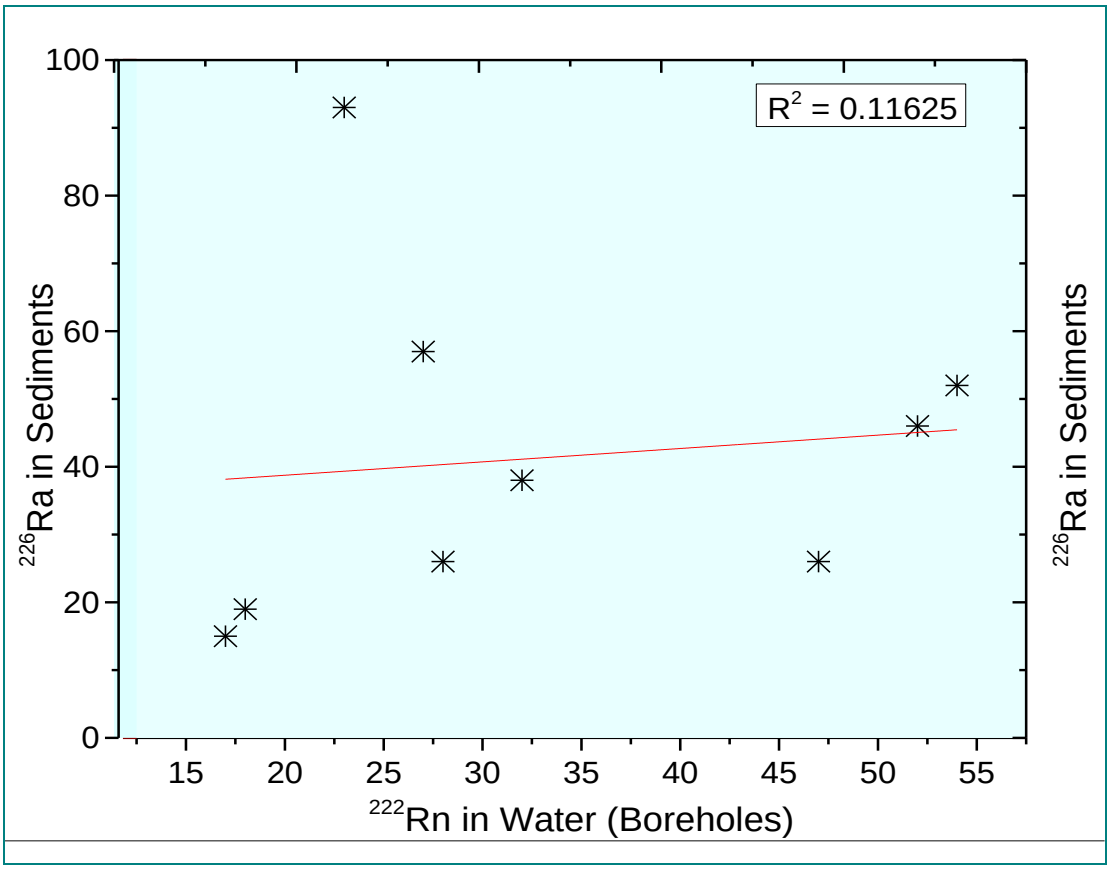


**Figure 5.12: Scatter plot with a linear fit for $^{222}$Rn in water (Boreholes) and $^{226}$Ra in sediments**

Figure 5.12 reports a positive correlation with a weak coefficient for radon in borehole water and radium in sediments sampled from the proximity of the sampled boreholes This was expected as radon isotopes dissolved in water is leached to underground sub-strums where their level is enhanced. Another possible reason for positive linearity in levels of radon in water and radium in sediments is that underground water lacks desorption of radon due to confinement. The time between collection and on-site analyses was maintained constant for both water from the well and water from boreholes.

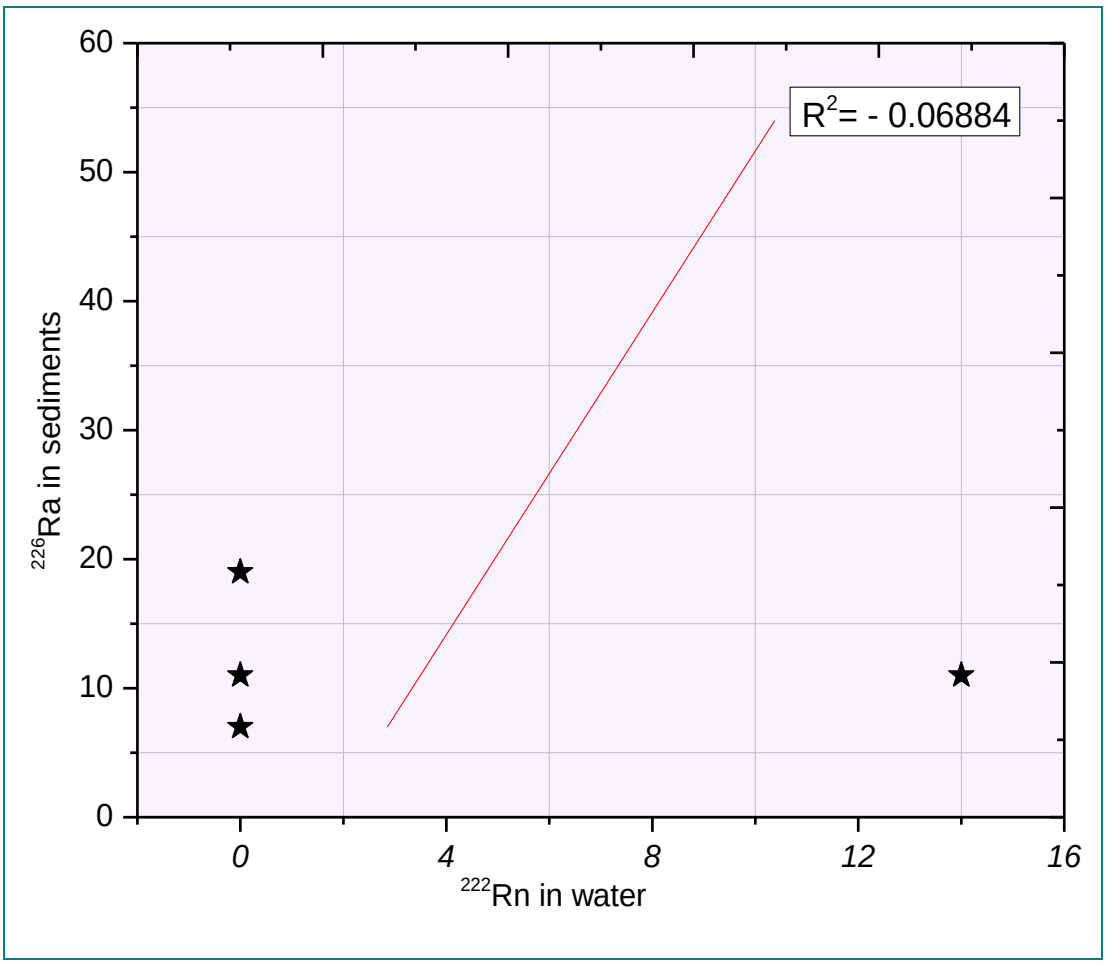


**Figure 5.13: Scatter plot for $^{222}$Rn in water versus $^{226}$Ra in sediments**

Figure 5.13 The correlational analysis correlation between the $^{222}$Rn levels in water and radium ($^{226}$Ra) in sediments from the geology of the sampled area reports a weak or no correlational relationship suggesting the radon levels in underground water are not directly related to the radium in the immediate geology.

### 5.6 Comparison of Present Work Findings with Previous Studies

The findings from this research were compared with data reported by similar surveys in different parts of Kenya and beyond. The range of radon activity in water in Bq $L^{-1}$ or kBq $m^{-3}$and the effective dose via ingestion were particularly compared with data from various data banks. The data on radium levels in sediments has similarly been compared

with geological data reported by other researchers in the area. Table 5.9 presents such comparisons.

**Table 5.11: Radon activity in water samples for this work and various other regions**

| Region | Radon Activity (Bq $l^{-1}$ ) | Reference |
|---|---|---|
| **Kenya (Kitui County)** | 30±1.5 $kBqm^{-3}$ | Present work |
| **Kenya (South Coast)** | 35.2±13.9 $Bqm^{-3}$ | Chege *et al.,* 2014 |
| **Kenya(various location)** | 37.1 ( Bq $l^{-1}$) | Mustapha *et al.*,2002 |
| **Nigeria** | 13.77 ± 1.05 $BqL^{-1}$ | Aruwa *et. al.*,2017 |
| **Pakistan** | 0.94 ± 0.05 $BqL^{-1}$ | Nasir *et. al.*,2012 |
| **India** | 4.42 $BqL^{-1}$ | Sudhir et al.,2016 |
| **Worlds Average** | 10 Bq $l^{-1}$ | USCEAR, 2000. |

**Table 5.12: Annual effective dose via ingestion of water for this work and various regions**

| Region | Effective Dose ($mSvy^{-1}$) | Reference |
|---|---|---|
| **Kenya (Kitui County)** | 0.006±0.0003 | Present work |
| **Kenya (Mrima hills)** | 1.7 | Chege *et al.,* 2014 |
| **Kenya (Kanana village)** | 0.03 | Chege *et al.,* 2014 |
| **Saudi Arabia** | 0.014.4 ± 0.8 | El-Araby *et al.,* 2019 |
| **Turkey** | 0.005 | Tabar *et al.,* 2014 |
| **Worlds average** | 1 | WHO,2004 |

In this present work, the radon concentration reported surpasses the world's average of 10 $BqL^{-1}$ (USCEAR, 2000). However, the levels of radon activity for this present work lie within the range of 4 – 40 $BqL^{-1}$ as recommended (UNSCEAR,2000) though much below as recommended levels100 $KBqm^{-3}$ (ICRP,2010; WHO,2009). The annual effective dose due to ingestion of water averaged 6.0 $\mu Svy^{-1}$ which is far below the recommended limit of 0.1 $mSvy^{-1}$ (EU, 2001; WHO, 2004) and the worldwide average of 1.15 $mSvy^{-1}$ as suggested by (UNSCEAR, 2000).

# CHAPTER SIX

## 6.0 CONCLUSION AND RECOMMENDATION

### 6.1 Conclusions

Radon levels in evaluated and the findings were compared with results reported in the existing literature. The survey reported a mean radon concentration of 30 ± 1.5 kBq $m^{-3}$ (30 ± 1.5 Bq/L) with a range of 0 - 120 ± 6 $kBqm^{-3}$. Regulatory bodies recommend a maximum radon concentration limit of 11 Bq/L USEPA, 1991. Based on the proposed limit, the current survey reports radon in water above 11.1 Bq/L. (UNSCEAR, 2000). The average radon activity from the borehole waters alone was 42±2.1 $kBqm^{-3}$, which is within the range of 200-600 $Bq/m^3$ suggested by the US-EPA 1999.

EU reports recommend remediation measure if the level of radon in water used for drinking purposes exceed an average of 100 $Bq/m^3$. Therefore, the average radon activity reported in this work is far below the given limit, thus the radiation doses via ingestion and inhalation emanating from the use of the sampled water sources pose no significant radiation threat.

The annual effective dose contributions to an individual consumer via ingestion of radon in water averaged 0.006±0.0003 $mSvy^{-1}$. The AED from radon and its daughters in water was well below the reference level of 0.1 $mSvy^{-1}$ recommended by US-EPA. The dose contribution arising from the release of $^{222}Rn$ in water to the air was found to be in reasonable range with the findings reported by previous similar surveys. The mean annual effective dose from water taken via inhalation suggests the use of water from these wells poses no significant radiological threat.

The study examined the presence of radionuclides in sediments collected within the locality of the boreholes. The study is necessary, as most radionuclides are soluble in water, thus high levels of radionuclides like $^{226}Ra$ in soils and rocks within the studied area may correspondingly suggest the presence and levels of radon in water. The levels of $^{226}Ra$ $^{232}Th$ and $^{40}K$ in sediments sampled within the locality of boreholes in Kitui County

were detectable. The findings reported an average of 41±2.07 Bq/Kg, 42±2.11 Bq/Kg and 860±43.01 Bq/Kg respectively.

The average activity levels of $^{226}Ra$ and $^{40}K$ were above the world's average of 33 Bq/Kg and 400 Bq/Kg respectively. $^{40}K$ was twice the world's average, which is in agreement with the existing literature as potassium has a high natural abundance in the crustal components. However, the activity level of $^{40}K$ was below the exemption level of 100,000 Bq/Kg suggested by ICRP, 2015. The mean absorbed dose averaged 82±4.13 nGy/h, which is above the world's mark of 60 nGy/h ICRP 2005. The annual effective dose rate averaged 0.2 ± 0.01 $mSv/y^{-1}$suggesting the sediments posed no significant harm to the population interacting with them.

The correlational analysis correlation between the $^{222}Rn$ levels in water and radium ($^{226}Ra$) in sediments from the geology of the sampled area reports a weak relationship suggesting the radon levels in underground water are not directly related to the radium in the immediate geology. Weak nonlinear correlation for radon levels in borehole water and sediments sampled from the corresponding borehole could be due to dissimilarities in the level (depths) in which the sediments were sampled, and the depth from which the water was sampled.

### 6.2 Recommendations

The study on radon was done during the dry season and since water evolves with prevailing climatic conditions and time, there is a need for consistent research throughout the year to establish a stable trend of the quality of the water consumed with time. In addition, there is a need for studying levels of radon during the rainy season to establish the correlation between times and dry periods.

High radon and radium levels in Mutha Ngosini springs of 120±6 kBqm-3 and 455±22 Bq/Kg respectively suggest there could be a rock vein enriched with granitic mineral accessories which need more radiologic surveys to establish consistent levels of radon in

water and radium in rocks and soils of the area. However, research-using samples collected from the surface soil is necessary.

Since studies on radon levels have not been done in the neighbouring sub-counties like Katulani, Ikutha and Mutito this study strongly recommends studies on radon more so for wells near rocky hilly areas where water oozes from granitic rocks, which has been associated with enhanced levels of radionuclides.

Since the major interaction of the population with the well is through the use of water from these wells, there was a need to test these elements direct in water which has been done.

This study strongly recommends a radiation pollution map for the water from dams, wells, underground, and soils for the entire County, as water requirements increase with populations increase.

## REFERENCES


Abu-Jarad, F., & Fremlin, J. H. (1983). Effect of internal wall covers on radon emanation inside houses. *Health Physics*, *44*(3), 243-248.

Abu, E ., Sharaf, M., Mansy, M., & Abbas, E. (1999). Natural radioactivity and radon exhalation rates in building materials used in Egypt. *Radiation Measurements*, *31*(1-6), 491-495.

Ahmed, M., Das, S., Haydar, M., Bhuiyan, M., Ali, M., Paul, D. J. J. o. N., & Physics, P. (2014). Study of Natural Radioactivity and Radiological Hazard of Sand, Sediment, and Soil Samples from Inani Beach, Cox's Bazar, Bangladesh. *4*(2), 69-78.

Ali, N., Khan, E. U., Akhter, P., Khan, F., & Waheed, A. (2010). Estimation of mean annual effective dose through radon concentration in the water and indoor air of Islamabad and Murree. *Radiation protection dosimetry*, *141*(2), 183-191.

Aruwa, A., Kassimu, A. A., Gyuk, P. M., Ahmadu, B., & Aniegbu, J. O. (2017). Studies on radon concentration in underground water of idah. *International Journal of Research Granthaalayah*, *5*(9), 266-75.

Bendibbie, M., David, M. & Jayanti, P. (2012). Multielemental Analysis of Limestone and Soil Samples of Kitui South (Kenya) Limestone Deposits. *International Journal of Fundamental Physical Sciences*, 2(4), 48-51

Beretka, J., & Matthew, P. J. H. p. (1985). Natural radioactivity of Australian building materials, industrial wastes and by-products. *48*(1), 87-95.

Chege, M. W. (2014). *Modelling Radon and Thoron Exhalation and Measurement of Total Natural Radiation Exposure in Mrima Hill, Kenya*. Published PhD Thesis, Kenyatta University Press.

Chege, M., Hashim, N., Nyambura, C., Mustapha, A., Hosada, M., & Tokonami, S. (2019). Radon and Thoron; Radioactive gases lurking in earthen houses in rural Kenya. *Frontiers in public health*, *7*, 113.

Choubey, V. M., & Ramola, R. C. (2001). Correlation between geology and radon levels in groundwater, soil and indoor air in Bhilangana Valley, Garhwal Himalaya, India. *Environmental Geology*, *32*(4), 258-262.

Choubey, V. M., Bartarya, S. K., Saini, N. K., & Ramola, R. C. (2005). Radon measurements in groundwater of inter-montane Doonvalley, Outer Himalaya: effects of geohydrology and neotectonic activity. *Environ Geol*, *40*(3), 257-266.

Cothern, C. R., Smith, J. E., & Smith Jr, J. E. (Eds.). (1987). *Environmental radon* (Vol. 35). Springer Science & Business Media.

Das, A., & Ferbel, T. (2003). *Introduction to nuclear and particle physics*. World Scientific.

Deka, P.C., et al 2001. Measurement of indoor radon progeny in some dwellings of Nothern Kamrup in Brahmaputra varlley region of Assam .2001. indian journal of environtal protection.,21:24-28.

Devaney, J. J. (1953). Theory of Alpha Decay. I. *Physical Review*, *91*(3), 587.

D. Halliday, Introductory Nuclear Physics, New York, John Wiley & Sons, Inc., QC 173 H18I. Kaplan, Nuclear Physics, Cambridge, Mass., Addison-Wesley Publishing Co., Inc.QC 173 K17.

Dodson, R. G (1953). **A** Geology of South-East Machakos area. *Geol. Surv. Kenya. Report No. 25: pp.3*

Duggal, V., Mehra, R., & Rani, A. (2013). Determination of 222Rn level in groundwater using a RAD7 detector in the Bathinda district of Punjab, India. *Radiation protection dosimetry*, *156*(2), 239-245.

Ebaid, Y. J. R. J. P. (2010). Use of gamma-ray spectrometry for uranium isotopic analysis in environmental samples. *55*(1-2), 69-74.

El-Araby, E. H., Soliman, H. A., & Abo-Elmagd, M. (2019). Measurement of radon levels in water and the associated health hazards in Jazan, Saudi Arabia. *Journal of Radiation Research and Applied Sciences*, *12*(1), 31-36.

Elijah, k. (2016). *Radioactivity concentrations and dose assessment for soil samples from wheat plantation areas of Narok County, Kenya* (Doctoral dissertation, Kenyatta University).

EPA (2002). Radionuclides in Drinking Water: A Small Entity Compliance Guide. USA

European Commission (2001) Commission Recommendation on the protection of the public against exposure to radon in drinking water supplies (2001/928/Euratom). Official journal of the European communities.

Faanu, A., Adukpo, O. K., Tettey-Larbi, L., Lawluvi, H., Kpeglo, D. O., Darko, E. O., & Efa, A. O. (2016). Natural radioactivity levels in soils, rocks and water at a mining concession of Perseus gold mine and surrounding towns in Central Region of Ghana. *SpringerPlus*, *5*(1), 98

Furusawa, Y., Nagai, S., Hirano, A., Ippommatsu, M., Aosaki, K., Yamada, K., & Akasaki, I. (2014). Development of under filling and encapsulation for deep-ultraviolet LEDs. *Applied Physics Express*, *8*(1), 012101.

Gamow, G. (1928). Zur quantentheorie des atomkernes. *Zeitschrift für Physik*, *51*(3-4), 204-212.

Gilmore, G. (2008). *Practical gamma-ray spectroscopy*. John Wiley & Sons.

Gilmore, R. S., Black, R. D., Arthur, S. D., Lewis, N., Hall, E. L., & Lillquist, R. D. (1988). Silicon and silicon dioxide thermal bonding for silicon-on-insulator applications. *Journal of applied physics*, *63*(8), 2773-2777.

Halime Kayakökü, Şule Karatepe, Mahmut Doğru (*2016*). "Measurements of radioactivity and dose assessments in some building materials in Bitlis, Turkey", *Applied Radiation and Isotopes.*

Hall, J.,Qian, X., Allada, K., Dutta, C., Huang, J., Katich, J., ... & Wang, Y., (2011). Single Spin Asymmetries in Charged Pion Production from Semi-Inclusive Deep Inelastic Scattering on a Transversely Polarized He 3 Target at Q 2= 1.4–2.7 GeV 2. *Physical Review Letters*, *107*(7), 072003.

Herman, G. T. (2019). 10 Iterative reconstruction techniques and their superiorization for the inversion of the Radon transform. *The Radon Transform: The First 100 Years and Beyond*, *22*, 217.

Hopke PK, Borak TB, Doull J, Cleaver JE, Eckerman KF, Gundersen LCS, Harley NH, Hess CT, Kinner NE, Kopecky KJ, Mckone TE, Sexton RG, Simon SL (2000) Health risks due to radon in drinking water. Environ Sci Technol 34:921–926.

IAEA., & IAEA. (2010). *Handbook of parameter values for the prediction of radionuclide transfer in terrestrial and freshwater environments*: International Atomic Energy Agency.

ICRP (1991). Annual limits on the intake of radionuclides by workers based on 1990 recommendations. International Commission of Radiological Protection, 66: Annals of the ICRP 21 (4).

ICRP. (2005). Low-dose Extrapolation of Radiation-related cancer risks. . *International Commission on Radiological Protection. Oxford: Pentagon press.*

International Commission on Radiation Protection (ICRP), (2015). Protection of the public in situations of prolonged radiation exposure ICRP Publication 82; Ann. ICRP 29 (1–2), Pergamon Press, Oxford.

International Commission on Radiological Protection (ICRP), (2005). Low-dose Extrapolation of Radiation-related cancer risks. ICRP 2005. Oxford: Pentagon press.

Kaplan, I. (1962). Nuclear physics (pp. 197—442). *Reading, Mass: Addison—wisely*.

Kebwaro, M. J. (2011). Gamma-ray spectrometry analysis of the surface soil around Mrima hill, Kenya Using NaI (TI) detector and decomposition technique. *M.Sc. thesis at* Kenyatta University, Kenya.

Kenya National Bureau of Statistics. (2019). The population of Lurambi sub-county. Retrieved from https://www.knbs.or.ke.

Koech Nehemiah Kipkirui (2017). Analysis of heavy metals, minerals and radionuclides in heavy sands from Tiva and Mwita Syano rivers, Kitui County. *M.Sc Thesis.*

Krane, Kenneth S., and Chichester W. (1988). Introductory nuclear physics, New York. ISBN: 047180553X.

Lapp, R.E. and Andrews, H.L. (1972), Nuclear Radiation Physics (4th edition), London: Sir Isaac Pitman and Sons Ltd.

Lilley J. S., Wiley (2001). Nuclear Physics: Principles and Applications.

Lilley, J. S., (2001) Nuclear Physics, New York, John Wiley & Sons Ltd., ISBN: 0-471-97936-8. Ltd., 2000, ISBN: 0-471-07338-5.

Matsitsi, S. M., Linturi, J. M., Kebwaro, J. M., & Kirago, L. M. (2020). Radiometric survey of the Tyaa river sand mine in Kitui, Kenya. *Radiation Protection Dosimetry*.

Matsitsi, S.M., Linturi, J. M., Kebwaro, J., Maweu, O.M. (2019). Effects of Seasonal Change on Levels of Geogenic Radionuclides in Sand and Rocks from Tyaa River deposit in Kitui County. *International Journal of Fundamental Physical Sciences (IJFPS), 9(1),14-19.* https://doi.org/10.14331/ijfps.2019.330124.

Monnin, M. M., & Seidell, L. (1997). 1.3 Radon Measurement Techniques. *Radon Measurements by Etched Track Detectors: Applications in Radiation Protection, Earth Sciences and the Environment*, 51.

Mustapha, A. O., Patel, J. P., & Rathore, I. V. S. (2002). Preliminary report on radon concentration in drinking water and indoor air in Kenya. *Environmental Geochemistry and Health*, *24*(4), 387-396.

Mustapha, A. O., Patel, J., & Rathore, I. J. R. p. d. (1999). Assessment of human exposures to natural sources of radiation in Kenya. *82*(4), 285-292.

Mutungi, M. J. (2018). Assessment of Natural Radio Activity Concentration Levels in Geological Samples Collected In Selected Areas in Makueni County.

Nasir, T., & Shah, M. (2012). Measurement of annual effective doses of radon from drinking water and dwellings by CR-39 track detectors in Kulachi City of Pakistan. *Journal OF Basic & Applied Sciences*, *8*, 528-536.

NCRP 1999 Biological effects and exposure limits for 'hot particles' *NCRP Report No. 130.*

Nugraha, E. D., Hosoda, M., Winarni, I. D., Prihantoro, A., Suzuki, T., Tamakuma, Y., ... & Tokonami, S. (2020). Dose assessment of radium-226 in drinking water from mamuju, a high background radiation area of Indonesia. *Radiation Environment and Medicine*, *9*(2), 79-83.

Nugraha, E. D., Hosoda, M., Mellawati, J., Untara, U., Rosianna, I., Tamakuma, Y., ... & Tokonami, S. (2021). Radon Activity Concentrations in Natural Hot Spring Water: Dose Assessment and Health Perspective. IJERPH 2021, 18, 920. *Assessment of Environmental Radioactivity and Radiation for Human Health Risk*, 99.

Nwankwo, L. I. (2013). Determination of natural radioactivity in groundwater in Tanke-Ilorin, Nigeria. *West African Journal of Applied Ecology*, *21*(1), 111-120.

Nyamai, C. M., Mathu, E. M., Opiyo-Akech. N., & Wallbrecher. E. (2003). A Re-appraisal of the Geology, Geochemistry, Structures, and Tectonics of the Mozambique belt in Kenya, East of the Rift System. *African Journal of Science and Technology (AJST), 4*, 51-71.

Patel, J. P (1991). Environmental radiation survey of the area of high natural radioactivity of Mrima hill of Kenya. *Discovery and innovation 3(3): pp. 31-36.*

Rani, A., Mehra, R., & Duggal, V. (2013). Radon monitoring in groundwater samples from some areas of northern Rajasthan, India, using a RAD7 detector. *Radiation protection dosimetry*, *153*(4), 496-501.

Reguigui, N. (2006). Gamma Ray Spectrometry. *Practical Information*.

Saha G.B, (2013) *Physics and Radiobiology of Nuclear Medicine*, DOI 10.1007/978-1-4614-4012-3.Media New York.

Sudhir. M., Rani, A., & Mehra, R. (2016). Estimation of radon concentration in soil and groundwater samples of Northern Rajasthan, India. *Journal of Radiation Research and Applied Sciences*, *9*(2), 125-130.

Tabar E, Kumru MN, I˙c¸hedef M, Sac¸ MM (2013) Radioactivity level and the measurement of soil gas radon concentration in Dikili geothermal area, Turkey. Int J Radiat Res 11(4):253–261.

Tabar, E., & Yakut, H. (2014). Radon measurements in water samples from the thermal springs of Yalova basin, Turkey. *Journal of Radioanalytical and Nuclear Chemistry*, *299*(1), 311-319.

Thabayneh, K. M., & Jazzar, M. M. (2012). Natural radioactivity levels and estimation of radiation exposure in environmental soil samples from Tulkarem Province-Palestine. *Open Journal of Soil Science*, *2*(01), 7.

U.S. Environmental Protection Agency (2003). Interim primary drinking water regulations - promulgation of regulations on radionuclides: *Federal Register*, v. 41, July 9, 1976, Part II, p. 28,402-29,409.

United Nations Scientific Committee on the Effect of Atomic Radiation (UNSCEAR) (2000). The general assembly with scientific annex. UNSCEAR, New York.

UNSCEAR (1993). United Nations Committee on Effects of Atomic Radiation. Exposure from natural sources of radiation. United Nations, New York.

UNSCEAR (2000). *Report to the general assembly with scientific annexes* (pp. 97e105). New York: United Nations. Annexure B.

UNSCEAR (2002), *Report of the United Nations Scientific Committee on the Effects of Atomic Radiation (UNSCEAR) 2002*, UN, New York, https://doi.org/10.18356/3b115807-en.

UNSCEAR (2005), *Report of the United Nations Scientific Committee on the Effects of Atomic Radiation (UNSCEAR) 2005*, UN, New York, https://doi.org/10.18356/f67bb874-en.

UNSCEAR (2010). *Report of the United Nations Scientific Committee on the Effects of Atomic Radiation on the Effects of Atomic Radiation*, 2010.

UNSCEAR, Sources and Effects of Ionizing Radiatic (United Nations, New York). 1993

UNSCEAR. (1988). Sources of ionizing radiation. United Nations Scientific Committee on Effects of Atomic Radiation 2000 report, United Nations, New York. 565-571.

UNSCEAR. (2000). United Nations Scientific Committee on the Effects of Atomic Radiation. Sources, effects, and risks of ionization radiation Report to The General Assembly, with Scientific Annexes B: Exposures from Natural Radiation Sources. 453-487.

UNSCEAR. (2008). United Nations Scientific Committee on the effect of Atomic Radiation report to the general assembly. *Annex B: exposures of the public and workers from various sources of radiation*.

UNSCEAR. (2010). Sources and effects of ionizing radiation. Report to the General Assembly, with scientific annexes. New York: United Nations.

US EPA (1999) Radon in drinking water health risk reduction and cost analysis. Fed Reg 64(38):9560–9599.

US-EPA United States Environmental Protection Agency (1991) National primary drinking water regulations for radionuclides. Federal Register: 33050-33127.

Varley, N. R. and Flowers, A. G (1998). Indoor radon prediction from soil gas measurements. *Health Physics. 74: 714-718.*

Wanjala, F. O., Otwoma, D., Kitao, T. F., & Hashim, N. O. (2015). Assessment of Natural Radioactivity and its Radiological Impact in Ortum Region in Kenya.

Wanjala, F. O., Hashim, N. O., Otwoma, D., Kebwaro, J., Chege, M., Nyambura, C., & Carmen, A. (2021). Lung Cancer Risk Assessment due to Radon and Thoron Exposure in Dwellings in Ortum, Kenya. *Journal of Environment Pollution and Human Health*, *9*(2), 64-70.

WHO (2008) Guidelines for third edition recommendations drinking-water quality, vol 1. World Health Organization, Geneva.

WHO (2009) handbook on indoor radon. A public health perspective. World Health Organization, Geneva, Switzerland.

Winde, F., & Wade, P. W. (2006). An Assessment of Sources, Pathways, Mechanisms and Risks of Current and Potential Future Pollution of Water and Sediments in Gold-mining Areas of the Wonderfonteinspruit Catchment: Report to the Water Research Commission. Water Research Commission.

World Health Organization (WHO) (2004) Guidelines for drinking water quality: radiological aspects

**APPENDIX 1**

Assembling RAD 7 Alpha detector in the field for Radon measurements

**APPENDIX 2**

Water sample collection with the help of research assistant

**APPENDIX 3**

Research assistant siphoning water to collection bucket where vial is filled

**APPENDIX 4**

Local residents fetching tap water from water kiosk in Mutha borehole

**APPENDIX 5**

Researcher collecting water bulk water sample using bucket from a borehole in Mutomo area